Oxide Surfaces
D.P. Woodruff, editor

Chapter 8

Molecules on well-structured oxide surfaces

H.-J. Freund, H. Kuhlenbeck, and T. Risse

Fritz Haber Institute of the Max Planck Society, Department of Chemical Physics, Faradayweg 4-6, 14195 Berlin, Germany

1. INTRODUCTION

Oxide surfaces under ultrahigh vacuum conditions are thermodynamically not well defined, due to the absence of a gas phase [1]. However, it is possible to kinetically stabilize the surfaces by forming thin films on metallic substrates, or by cleavage of single crystals in vacuum, and by keeping the temperature of the system below the threshold for oxygen vacancy formation. These surfaces can be investigated by surface science techniques. The literature contains books and several review articles on such systems [2-14]. We will focus on some specific aspects of geometric and electronic structure concerning the interaction of molecules with oxide surfaces.

We discuss a variety of cases: MgO(100) and NiO(100) surfaces are examples for bulk terminated non-polar surfaces of rocksalt-type crystals with very moderate relaxations of the interlayer spacings. Cr_2O_3(0001) and V_2O_3(0001) surfaces are depolarized polar surfaces of corundum type materials with strong relaxations several layers down into the bulk. TiO_2(110), RuO_2(110) and VO_2(110) surfaces are intermediate cases. The V_2O_5(0001) surface is an example for a layered oxide structure. The electronic structure of these surfaces has been investigated by various electron spectroscopic methods resulting in a deeper understanding of the "ideal", i.e. defect "free" surfaces, giving us a reference point to address the question of defect formation and defect structure.

Several adsorption studies on probe molecules such as CO, NO, CO_2, H_2O, H_2 and O_2 have been undertaken. Here we mention the remarkable differences we find for CO adsorption on rocksalt (100) and corundum (0001) surfaces. While CO stands upright - as expected – with the carbon end pointing to the substrate on NiO(100) it lies almost flat on Cr_2O_3(0001) and V_2O_3(0001). We show, that while the adsorption energies are similar in both cases, CO as a probe molecule reacts strongly towards differences in the electric field distributions on the surfaces. The experimental observations are complemented with theoretical

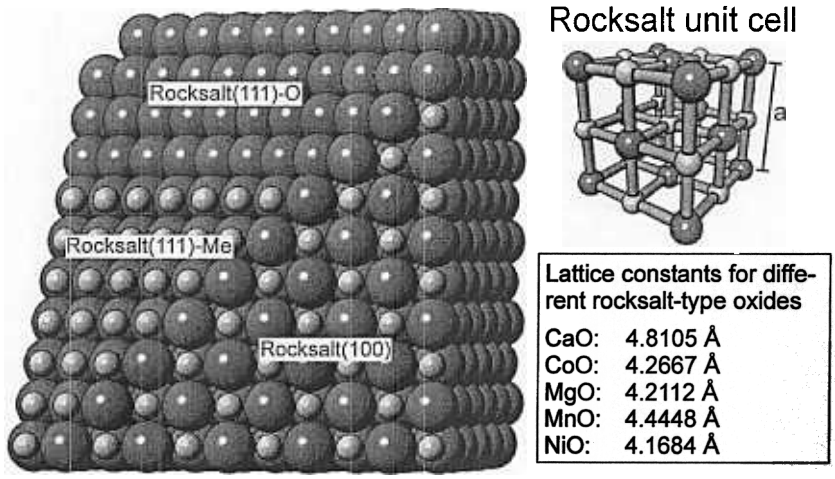

Fig. 1. Structure of rocksalt oxides. Lattice constants from [15].

considerations in order to address and rationalize details of the molecule surface bonding.

Another remarkable issue concerns the adsorption and dissociation of molecular oxygen on oxide surfaces. When such surfaces are metal terminated in UHV, the dissociative adsorption of oxygen may lead to oxygen terminations, very different from bulk terminations. This is exemplified for the case of $Cr_2O_3(0001)$.

Special techniques in surface science to study molecular motion in adsorbed layers are a problem that has found little attention in surface science, even though it is of utmost importance. Electron spin resonance is one such method. We discuss diffusion of NO_2, rotational motion of $((CH_3)_3C)_2NO$ and melting of self-assembled layers of spin-labeled fatty acids adsorbed on $Al_2O_3(0001)$.

2. SURFACES OF OXIDES WITH ROCKSALT STRUCTURE

Fig. 1 shows the rocksalt lattice [15]. We will discuss MgO and NiO as limiting cases of oxides, one containing a simple metal ion and the other one a transition metal ion. The (100) surface of such a material represents a non-polar surface, the (111) surface represents a polar oxide surface. Since the lattice constants are very similar for both oxides (MgO: 4.21 Å, NiO: 4.17 Å) [15], we expect the surface structures to be similar. The non-polar surface exhibits a nearly bulk terminated surface as shown in Fig. 2a and it is very similar for both materials. We have put together information from LEED [16-21] and STM [22-25] analysis. There is very small interlayer relaxation and only a small rumpling of the surface atoms, whereby the larger anions move outwards and the small cations very slightly inward. A completely different situation is encountered for the polar (111) surfaces. Due to the divergent surface potential [13] on an ideally, bulk terminated polar surface, the surface reconstructs and exhibits a so

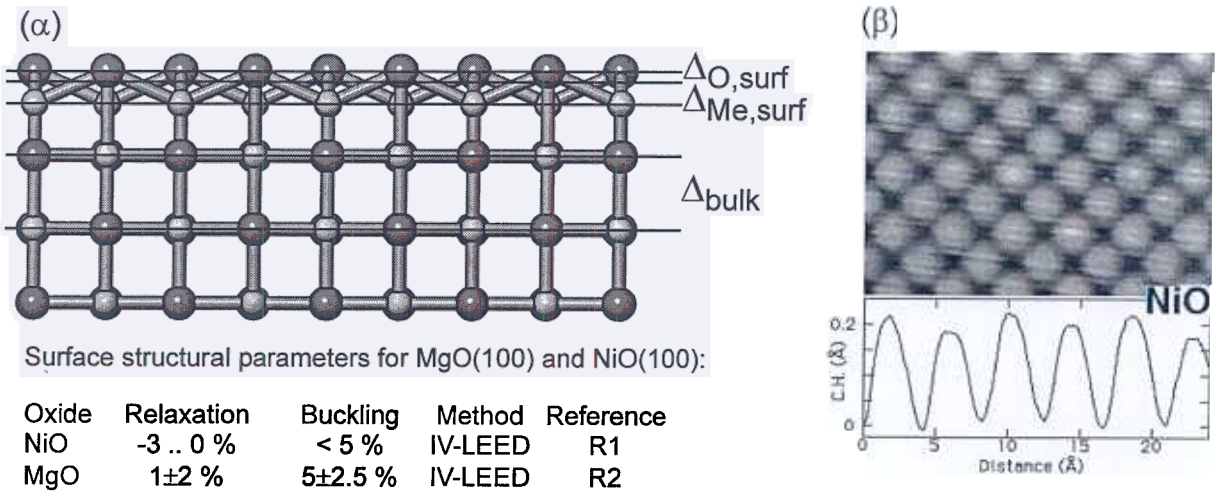

Surface structural parameters for MgO(100) and NiO(100):

Oxide	Relaxation	Buckling	Method	Reference
NiO	-3 .. 0 %	< 5 %	IV-LEED	R1
MgO	1±2 %	5±2.5 %	IV-LEED	R2
MgO	-0.56±0.35 %	1.07±0.5 %	GIXS	R3

Buckling: $\Delta_{O,surf} - \Delta_{Me,surf}$
Relaxation: $\Delta_{bulk}-(\Delta_{O,surf} + \Delta_{Me,surf})/2$

Fig. 2a. (α): Model for buckled surfaces of oxides with rocksalt structure and some experimental results for the surfaces of NiO(100) and MgO(100) (R1: ref. [21], R2: ref. [17], R3: ref. [34]). (β): STM image of a UHV-cleaved NiO(100) surface [25]. V_{sample} = 1.3 V, I_{tunnel} = 1.0 nA.

called octopolar reconstruction or even a mesoscopic facetting as opposed to the nanofacets in the case of the octopolar reconstruction [26, 27]. The structural and morphological evidences based on LEED [28], GIXD [29-31], STM [32] and electron microscopy [33] are collected in Fig. 2b. The data reported so far suggest that the d-electrons of the transition metal ion have a very small influence on structural parameters.

Before we proceed to a more detailed discussion of the binding of adsorbed molecules, a few remarks concerning the electronic structure of oxide surfaces are appropriate. Early on, Stefan Hüfner and coworkers have investigated the electronic structure of transition metal bulk samples and a great deal has been learned [35, 36]. There have also been attempts to investigate the surfaces of these materials with respect to electronic structure, notably in the recent work by Noguera and Mackrodt [37, 38]. Qualitatively, it was expected that, due to the high ionicity of some compounds, there are pronounced surface effects. Photoelectron spectroscopy has been used to experimentally verify these expectations through the detection of chemically shifted core levels. However, the shifts are not large enough to be detectable due to the relatively complex satellite structure accompanying metal core ionization [36]. Eventually, this was also rationalized via more sophisticated quantitative calculations which showed that there are several compensating contributions rendering the surface fields only slightly different from the bulk. Applying techniques allowing for higher energy resolution have then clearly demonstrated surface effects. In the

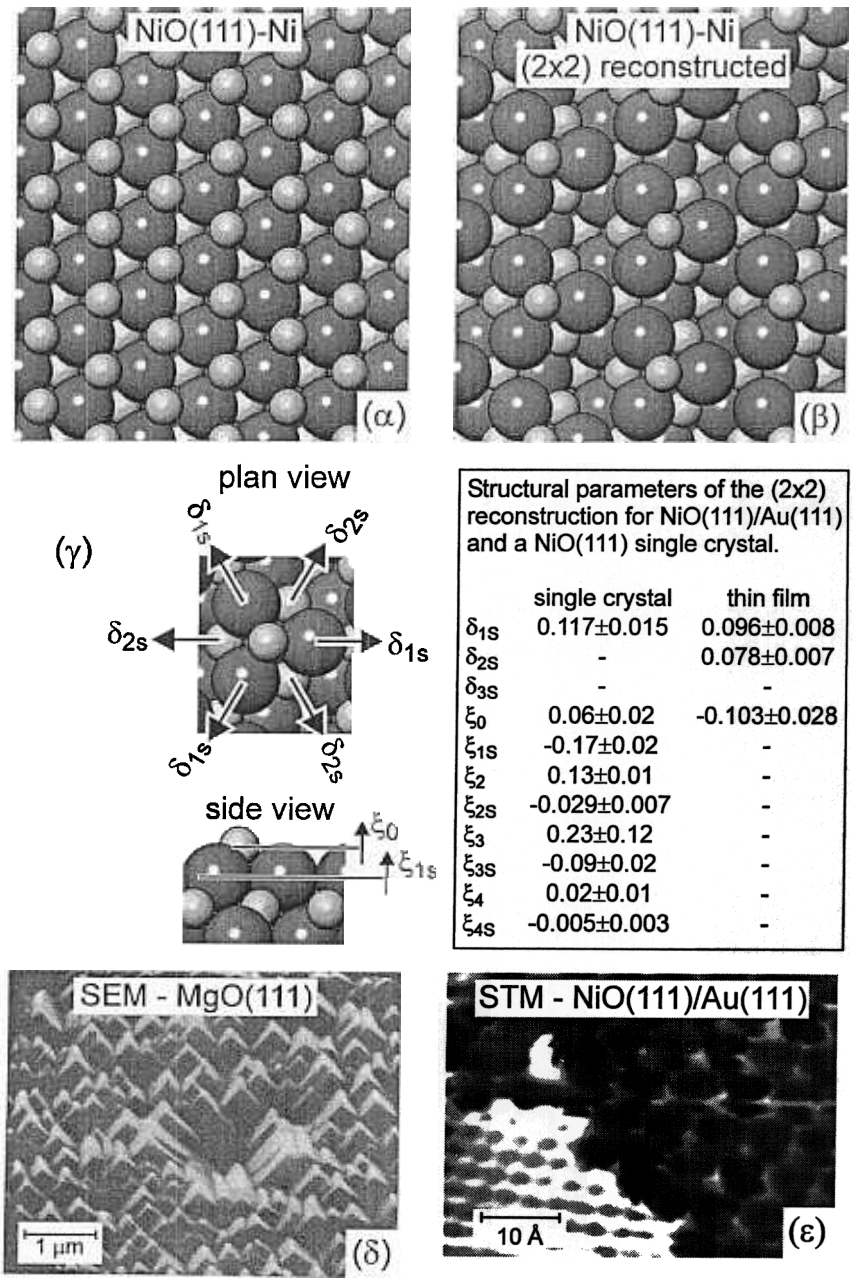

Fig. 2b. (α), (β): Models for the bulk-terminated and the (2×2) reconstructed NiO(111) surface. In both images the surfaces are terminated by nickel atoms. (γ): Structural parameters for the (2×2) reconstructions of NiO(111) and NiO(111)/Au(111) determined with grazing incidence X-ray scattering [31]. The meaning of some of the parameters is schematically illustrated in the left part. ξ_n means a vertical displacement of the n^{th} layer, and δ_n a lateral displacement. If an s is added in the index then displacements correlated by symmetry are meant. For the single crystal surface only nickel termination was observed whereas for the thin film nickel and oxygen termination occur. (δ): SEM image of the MgO(111) surface after annealing at 1400 K for 1 min [33]. Large facets terminated by (100)-type surfaces are visible. (ε): STM image of a thin NiO(111) film on Au(111) recorded with a non-metallic tip apex [32]. U = -0.3 V, I = 0.5 nA. The dark part of the image is due to the (2×2) reconstruction whereas the bright part in the lower left corresponds to Au(111).

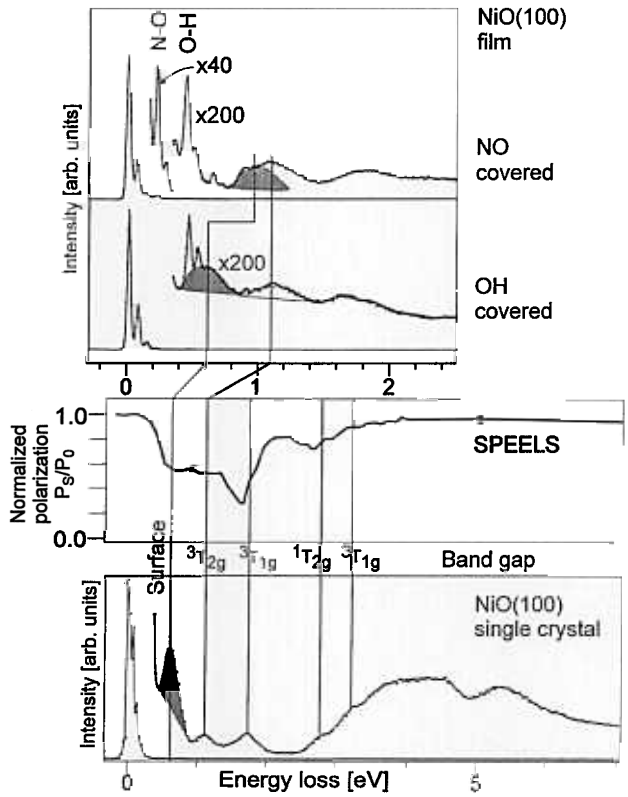

Fig. 3. Electron energy loss spectra of NiO(100) surfaces. Lower panel: clean NiO(100) surfaces, UHV-cleaved single crystal. The assignment of the features according to theory is given and supported by spin polarized measurements [44, 45]. Upper panel: adsorbate covered NiO(100) films. Lower trace: defects OH saturated, before NO adsorption; upper trace: after adsorption of NO [40].

Merz group [39] and our laboratory [40] electron energy loss spectroscopy (EELS) in the regime of electronic excitations has been used to identify excitations in the surface layer.

Fig. 3 shows a set of spectra taken on NiO(100) surfaces. The lowest trace has been taken on a clean single crystal. The broad features peaking at 4-5 eV correspond to charge-transfer excitations crossing the band gap of the insulating NiO bulk. In the gap there are narrow features due to excitations within the d-electron state manifold of the open shell Ni^{2+} ions. As the excitation energy within this manifold increases the number of states increases, so that near the charge-transfer band those states overlap and lead to the monotonous increase of intensity in this energy region. Most of the optically allowed transitions have been spectroscopically observed by transmission spectroscopy of bulk samples [41-43].

Bärbel Fromme and Eberhard Kisker have performed spin-polarized EELS measurements, which allow an assignment of the spin character of all states via the control of spin-polarization in the scattering conditions [44, 45]. The assignment and a spin-polarization measurement have been superimposed on the spectra. The important point here is that there are additional spectroscopic fea-

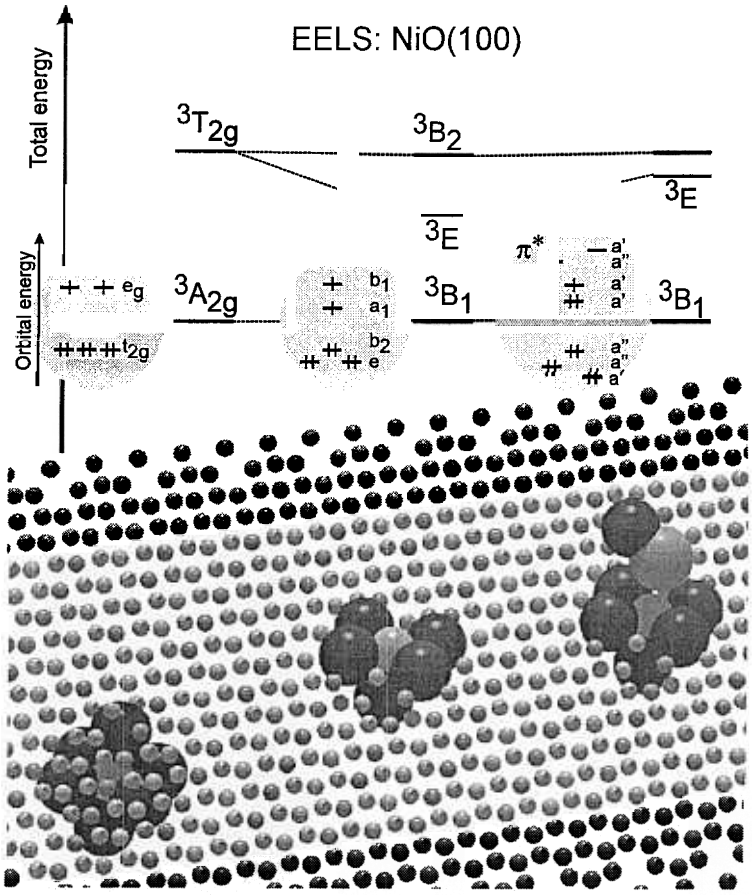

Fig. 4. Correlation of structural data with electronically excited states on NiO(100). Lower panel: (left) coordination of a Ni ion in the bulk, (middle) coordination of a Ni ion in the clean (100) surface as well as (right) in the case of adsorbed NO. Upper panel: orbital diagram and total energies from cluster calculations [40, 46].

tures, most pronounced at 0.6 eV excitation energy which are not due to excitations in the bulk but rather in the surface layer. This can be experimentally demonstrated by an adsorption study [40]. Those excitations localized in the surface should be most strongly affected by adsorbed species. The experiment has been performed on a thin film sample because the surface has to be cooled to adsorb an appreciable amount of NO in this case. It is very obvious that the peak at 0.6 eV is influenced. In fact, it is shifted towards the position of a feature originating from an excitation in the bulk. In passing we note that the NiO(100) film has been treated with water before the experiments had been performed, in order to saturate the defects with hydroxyls via dissociative adsorption of water. The vibrational losses caused by the hydroxyls are clearly visible before NO adsorption took place. NO adsorption then induces yet a further vibrational loss at lower loss energy.

What is the nature of the surface excitation and why is it different from the bulk excitation? Volker Staemmler and his group have performed ab-initio cluster calculations [40, 46], the result of which can be summarized as follows: Due to the localization of the Ni-d-electrons it is sufficient to consider a single

Ni^{2+} ion within its octahedral coordination sphere if we consider the situation encountered in the bulk (see Fig. 4). The ground state is a $^3A_{2g}$ state with two unpaired d-electrons in the e_g orbitals of the ligand field split set of d-orbitals. The first excited state results from an excitation from the completely filled t_{2g} subset into the partly filled e_g subset giving rise to an excitation located near 1 eV. There are many more higher excited states, some of which are assigned according to the work of Fromme et al. [44, 45].

In the surface, however, one of the coordinated oxygen ions is missing and the symmetry of the local Ni^{2+} site is reduced to C_{4v}. Consequently, the degenerated e_g subset is split. The t_{2g} subset is also split, but this effect is not so important. The d-orbital of the former e_g subset pointing along the Ni-O axis has lost part of its destabilizing interaction and, consequently, its energy decreases. The calculation shows that still both orbitals in the former e_g subset are singly occupied after reduction of symmetry. Therefore, the first excited state in a Ni^{2+} surface ion is at lower energy than in the bulk, as also revealed by the experiment.

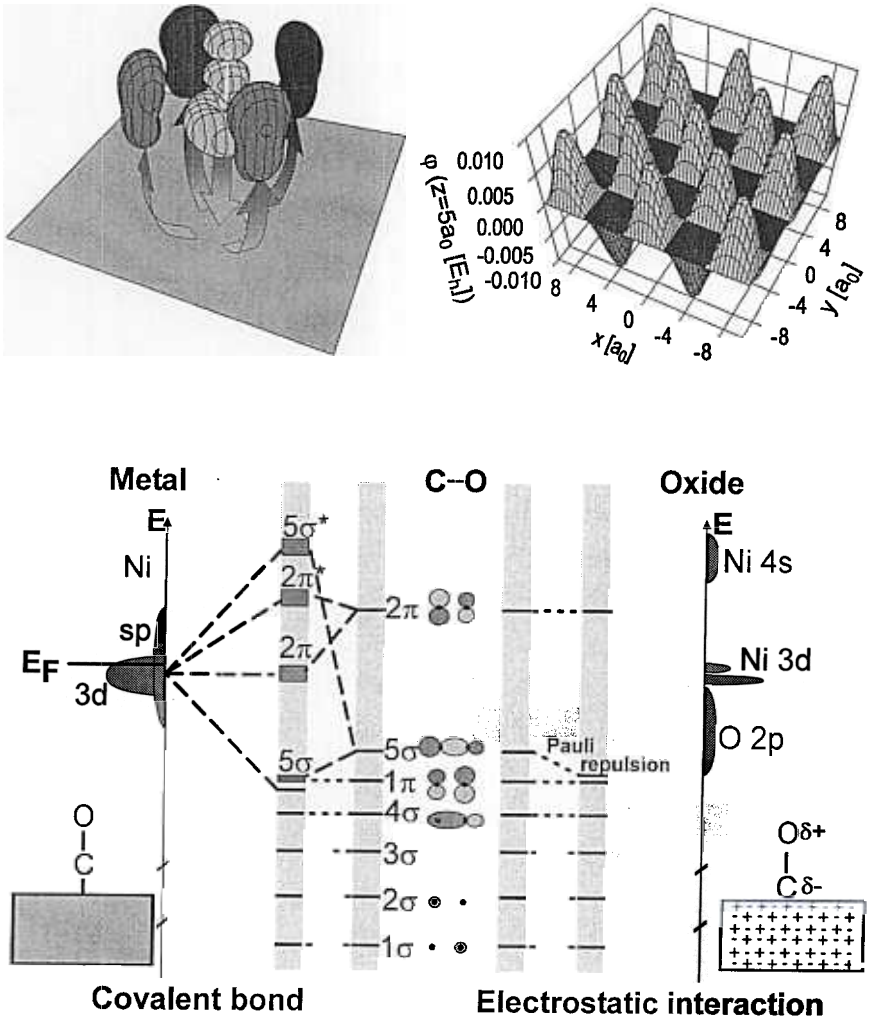

Fig. 5. Orbital diagram for the bonding of CO to Ni-metal (left) and to Ni-oxide (right).

If an NO molecule is now coordinated to the Ni^{2+} surface ion, the energetic position of the orbital is raised again, (similar to the presence of the sixth oxygen ion) effectively moving the excitation energy back close to the bulk position. It is clear from these results that the surface effect on the excitation energies is of the order of 0.4 eV, and thus the above mentioned lack of evidence from other techniques can be rationalized.

There has been an interesting attempt to look with EELS for the surface states at higher excitation energies at ~ 1 eV and 2.1 eV which have not been addressed here but have been mentioned by Freitag et al. [40] and discussed by Fromme et al. [44, 45]. Müller et al. [47] have varied the thickness of the NiO layer between one and several layers and determined the EELS spectra. This study supports the previous assignment of the peak at 0.6 eV to a surface state but they cannot find evidence for a surface state contribution at 1 eV. The authors argue that this may be due to cross section limitations under the chosen experimental conditions. They do find clear evidence for a surface contribution at 2.1 eV.

At this point we return to the question raised above, on the binding and interaction of molecules with oxide surfaces. Molecules bind to oxides via a bonding mechanism considerably different from metal surfaces. A CO molecule, for example, binds to metals via chemical bonds of varying strength involving charge exchanges [48]. Fig. 5 illustrates the bonding of CO to a Ni- metal atom via the so-called σ-donation/π-back-donation mechanism schematically on the basis of a one electron orbital diagram.

The σ- and π-interactions lead to a relative shift of those σ- and π-orbitals involved in the bond with respect to those orbitals not involved. The diagram reflects this via the correlation lines. This may be contrasted by the electrostatically dominated interaction between a CO molecule and a Ni ion in nickel-oxide [46, 49]. There is a noticeable σ-repulsion between the CO carbon lone pair and the oxide leading to a similar shift of the CO 5σ-orbital as in the case of the metal atom. However, there is no or little π-back-donation so that the CO π-orbitals are not modified [50, 51]. Conceptually, the situation is transparent and one would expect that a detailed calculation reveals the differences quantitatively. However, as it turns out the description by ab-initio calculations is very much involved and today a full account cannot be given [52].

Theoretically (Table 1) [46, 52-63], the prediction is that CO as well as NO bind very weakly to NiO [52]. The predicted binding energy of CO is of the order of 0.1 eV and it is expected to be similar to CO binding to MgO(100), i.e. the influence of the Ni d-electrons should be negligible [52].

To shed light on this problem it was necessary to perform thermal desorption measurements on cleaved single crystal surfaces, being the surfaces with the least number of defects [64]. In Figs. 6 and 7 TDS data for CO and NO on vacuum-cleaved NiO(100) are compared with data for thin NiO(100) films grown

by oxidation of Ni(100). At temperatures of 30 K and 56 K multilayer desorption for CO and NO, respectively, shows up. The pronounced features at higher temperatures correspond to desorption of the respective adsorbate at

Table 1. Literature data for adsorption of CO and NO on NiO(100) and MgO(100).

Author	System	Method	Adsorption energy (eV)
Pacchioni and Bagus [53]	CO/NiO(100)	ab-initio cluster calculation	0.24
Klüner [54]	NO/NiO(100)	ab-initio cluster calculation, BSSE correction	≈ 0
Pöhlchen and Staemmler [46]	CO/NiO(100)	ab-initio cluster calculation, BSSE correction	0.03 to 0.1
Cappus et al. [55]	CO/NiO(100)/Ni(100)	TDS, Redhead	0.32
Vesecky et al. [56]	CO/NiO(100)/Ni(100)	IRS, Clausius-Clapeyron	0.45
Staemmler [57]	NO/NiO(100)	ab-initio cluster calculation, BSSE correction	0.1
Pöhlchen [58]	NO/NiO(100)	ab-initio cluster calculation, BSSE correction	<0.23
Kuhlenbeck et al. [59]	NO/NiO(100)/Ni(100) and NO/NiO(100)	TDS, Redhead	0.52
Nygren and Pettersson [52]	CO/MgO(100)	ab-initio cluster calculation, BSSE correction	0.08
Chen et al. [60]	CO/MgO(100)	DFT	0.28
Neyman et al. [61]	CO/MgO(100)	DFT, BSSE correction	0.11
He et al. [62]	CO/MgO(100)/ Mo(100)	IRS, Clausius-Clapeyron, TDS, Redhead	0.43 0.46
Furuyama et al. [63]	CO/MgO powder	IRS, Clausius-Clapeyron	0.15 to 0.17

BSSE: Basis Set Superposition Error. TDS: Thermal Desorption Spectroscopy. DFT: Density Functional Theory. IRS: InfraRed Spectroscopy. Clausius-Clapeyron: evaluation of pressure and temperature dependent IR-intensities with the Clausius-Clapeyron equation. Redhead: evaluation of TDS data with the Redhead equation [65].

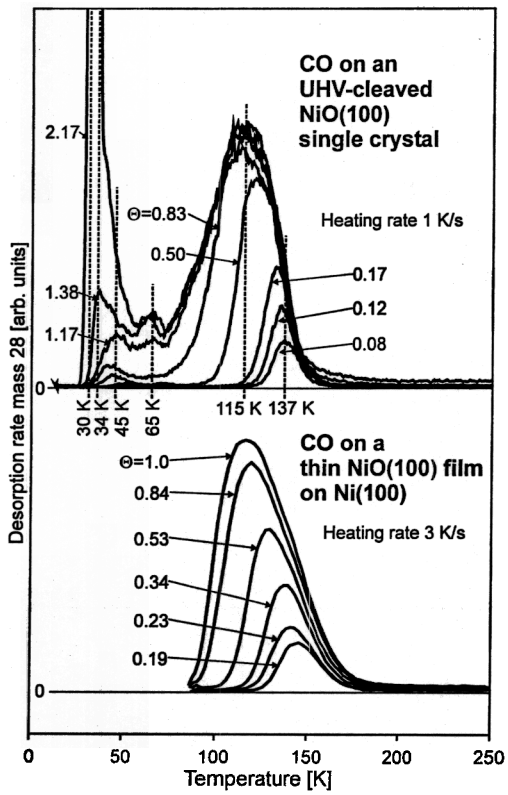

Fig. 6. Thermal desorption spectra of CO on NiO(100) cleaved in vacuum (upper part) and CO on a thin NiO(100) film grown by oxidation of Ni(100) (lower part). The mass spectrometer was set to mass 28 (CO). CO doses are given relative to the dose needed to prepare a monolayer.

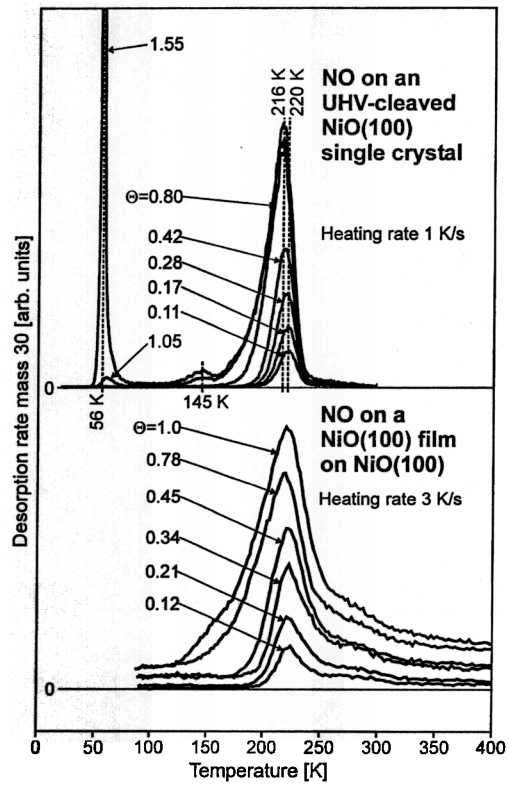

Fig. 7. Thermal desorption spectra of NO on NiO(100) cleaved in vacuum (upper part) and NO on a thin NiO(100) film grown by oxidation of Ni(100) (lower part). The mass spectrometer was set to mass 30 (NO). NO doses are given relative to the dose needed to prepare a monolayer.

(sub)monolayer coverage. In the case of the CO adsorbate at 34 K desorption of the second layer is found and the states at 45 K and 145 K for CO and NO, respectively, are due to adsorption on defects as concluded from data obtained from ion bombarded surfaces (not shown here). It is obvious that for both adsorbates the thin film data and the data of the cleaved samples agree well, in particular for NiO(100) the thin film data are comparable to those from the more perfect surfaces of the cleaved samples. The higher defect density of the thin film surfaces leads to small, but clearly visible additional peaks in the TDS data which show up as shoulders near to the main peak, for example in the NO spectra. Nevertheless, the general shapes of the thin film spectra of both adsorbates are very similar to those of the cleaved samples.

For CO the shift of the peak maximum with increasing coverage indicates that at higher coverage repulsive lateral interaction comes into play which may lead to occupation of energetically less favorable sites. This is not the case for the NO adsorbate which may be attributed to smaller lateral interactions and to the higher adsorption energy which makes adsorption more site specific, and thus may inhibit compression of the layer involving site changes.

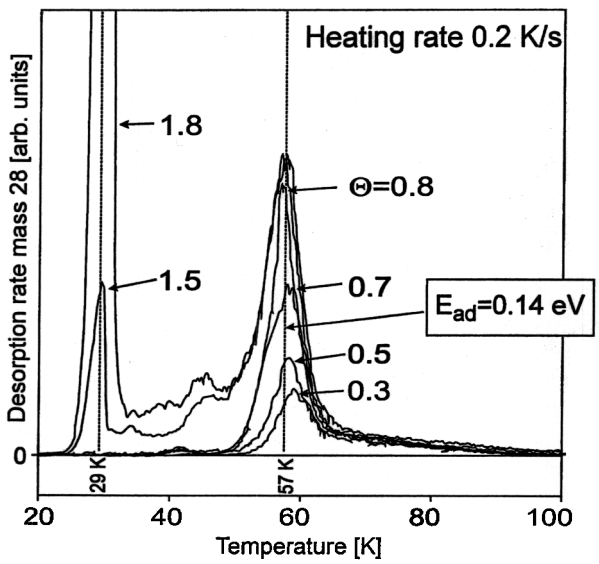

Fig. 8. Thermal desorption spectra of CO on MgO(100) cleaved in UHV. The mass spectrometer was set to mass 28 (CO). CO doses are given relative to the dose needed for the preparation of a monolayer.

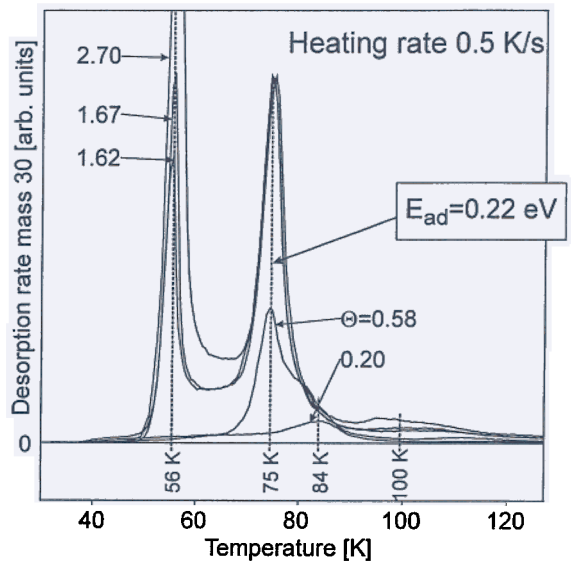

Fig. 9. Thermal desorption spectra of NO on MgO(100) cleaved in UHV. The mass spectrometer was set to mass 30 (NO). NO doses are given relative to the dose needed for the preparation of a monolayer.

TDS data for NO and CO on vacuum-cleaved MgO(100), for comparison, are plotted in Figs. 8 and 9. Multilayer desorption is found at 29 K and 56 K for CO and NO, respectively. The small features around 45 K and 100 K are likely due to defect adsorption since they saturate at rather low coverage. Desorption from layers with small coverage is found at 57 K and 84 K for CO and NO, respectively.

The data for CO and NO on NiO(100) have been evaluated using the leading edge method as well as a complete analysis. Details of the procedures may be found in [66, 67]. Both methods determine the heat of adsorption as a function of the coverage of molecules already on the surface. The results of the evaluation are shown in Figs. 10 and 11. Both graphs exhibit a trend which is generally to be expected for laterally interacting adsorbate layers: the adsorption energy decreases with increasing coverage. At coverages near to one monolayer the energies converge towards the multilayer values (0.09 eV and 0.18 eV for CO and NO, respectively [68]). At low coverage the lateral interactions are most likely small so that the corresponding adsorption energies may be compared with theoretical results since in the calculations lateral interactions have not been considered. As indicated in Figs. 10 and 11, the low coverage adsorption energies are

Table 2. Compilation of low-coverage bonding energies for NO and CO on NiO(100) and MgO(100) obtained in [10]

	NiO(100)	MgO(100)
CO	0.30 eV	0.14 eV
NO	0.57 eV	0.22 eV

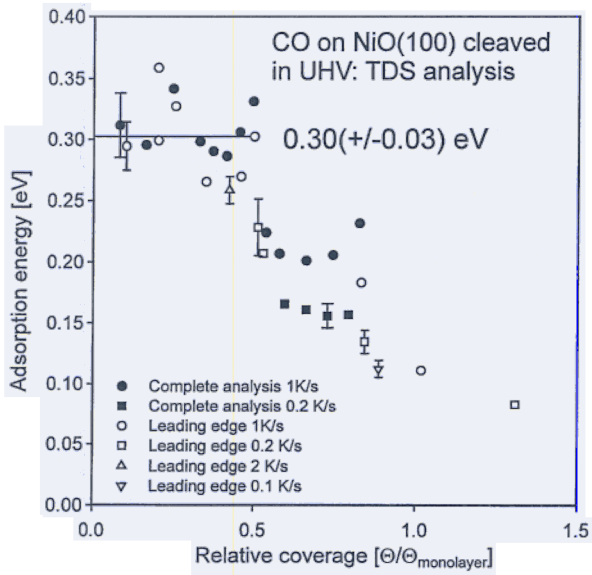

Fig. 10. Adsorption energy of CO on NiO(100) cleaved in vacuum as a function of coverage. The data have been determined from TDS spectra like those shown in Fig. 6 (upper part) using the leading edge method and complete analysis. TDS data taken with heating rates of 0.1, 0.2, 1 and 2 K/s have been used.

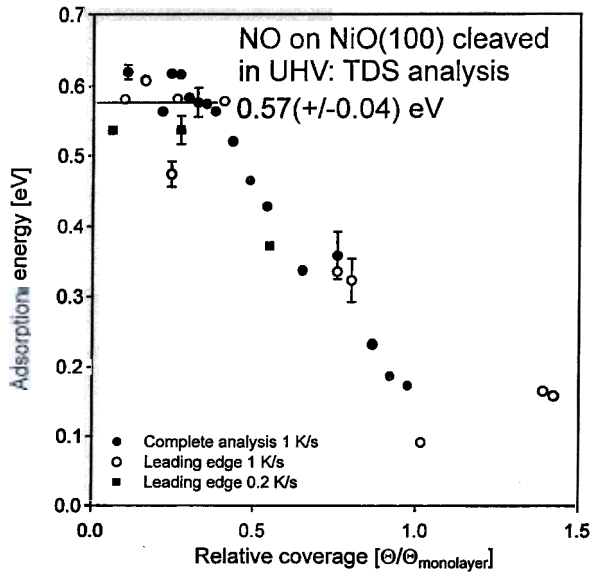

Fig. 11. Adsorption energy of NO on NiO(100) cleaved in vacuum as a function of coverage. The date have been determined from TDS spectra like those shown in Fig. 7 (upper part) using the leading edge method and complete analysis. TDS data taken with heating rates of 0.2 and 1 K/s have been used.

0.30 and 0.57 eV for CO and NO, respectively.

The low coverage adsorption energies for CO and NO on NiO(100) and MgO(100) are compiled in Table 2. According to theory the interaction of the adsorbates with MgO(100) and NiO(100) are expected to be similar since the bonding should be mainly electrostatic in nature [52] (the electric fields at the surfaces of NiO(100) and MgO(100) are similar). However, according to Table 2 the bonding energies are considerably different, with the higher values being obtained for NiO(100). Covalent interactions involving the Ni3d electrons may play a role for the adsorbate-substrate interaction which do not show up in the calculations published so far.

As far as it concerns the basis set superposition error (BSSE) corrected calculations listed in Table 1 which are expected to yield qualitatively better results as compared to the non-corrected calculations, it appears that the theoretical results for adsorption on MgO(100) are in general in line with our experimental results, whereas a similarly favorable comparison can not be made for NiO(100). It appears necessary to re-investigate the role of the Ni3d electrons in future theoretical studies.

The interaction between the molecule and the d-electrons of the substrate system is more obvious in the case of NO interaction with NiO. The molecule is tilted with respect to the surface normal as is experimentally evident from X-ray absorption measurements [59] as well as photoelectron diffraction investigations

by the Woodruff group [69]. The tilt angle is near 45-60° with the nitrogen end of the molecule pointing towards a Ni ion. The interatomic distance between N and O is near the one known from the free molecule, the separation from the surface Ni ion is determined to be 1.88 ± 0.2 Å. It was early pointed out by Staemmler and his group that this tilt is a consequence of the interaction of the unpaired electron on the NO moiety with the open shells on the Ni ion. A detailed discussion of the bonding mechanism can be found in ref. [57]. On MgO(100) preliminary calculations have indicated that the NO molecule is oriented perpendicular to the (100) surface plane. This appears to be reasonable in light of the missing d-electrons of the Mg ion. There are further indications for weak chemisorptive interactions between NO and the NiO(100) surface: Although there is only one NO species on the surface, the N1s photoelectron spectrum exhibits a broad band with two maxima. Such phenomena are connected with the dynamics of the screening processes accompanying the formation of the core hole. Detailed studies on screening phenomena have been reported for molecules on metal surfaces, [70-72], and it is well known, that systems with weak chemisorptive interactions exhibit the most complex line shapes. For weak chemisorption systems there is a high probability to find the final hole, both on the adsorbed molecule itself or, through extra molecular screening, on the substrate, giving rise to several final states, and thus to several intense components in the spectrum. It was proposed some time ago that such phenomena are also responsible for the line shapes observed for NO/NiO(100) [59]. The above mentioned recent photoelectron diffraction investigations have clearly demonstrated that the observed components in the N1s spectrum stem from a single species.

The adsorption of CO on MgO has been thoroughly investigated by Heidberg and his group using IR-spectroscopy [73] and by Weiss and Toennies using helium atom scattering spectroscopy (HAS) [74]. They have clearly demonstrated that CO develops ordered phases on the cleavage planes and that order and spectroscopic properties depend on the quality of the prepared surfaces. From their experiments the influence of the presence of surface defects on adsorption properties is very obvious but a quantitative evaluation based on the number and the nature of the defects has not been reported.

The quantitative evaluation of defects is a well defined but hard to tackle problem for future studies that has to be taken on by our research community. Water adsorption is an example that lends itself to a study of the influence of defects, because at lower coverage the (100) cleavage planes of MgO and NiO do not dissociate water, while the presence of defects does induce water dissociation.

Water adsorption on MgO(100) is the best studied system so far [64, 75-77]. The groups of Heidberg [75], Weiss and Toennies [76] have studied it with IR, LEED and HAS. While these groups have used surfaces prepared through in situ cleavage, Stirniman et al. [78] have employed bulk single crystals prepared via

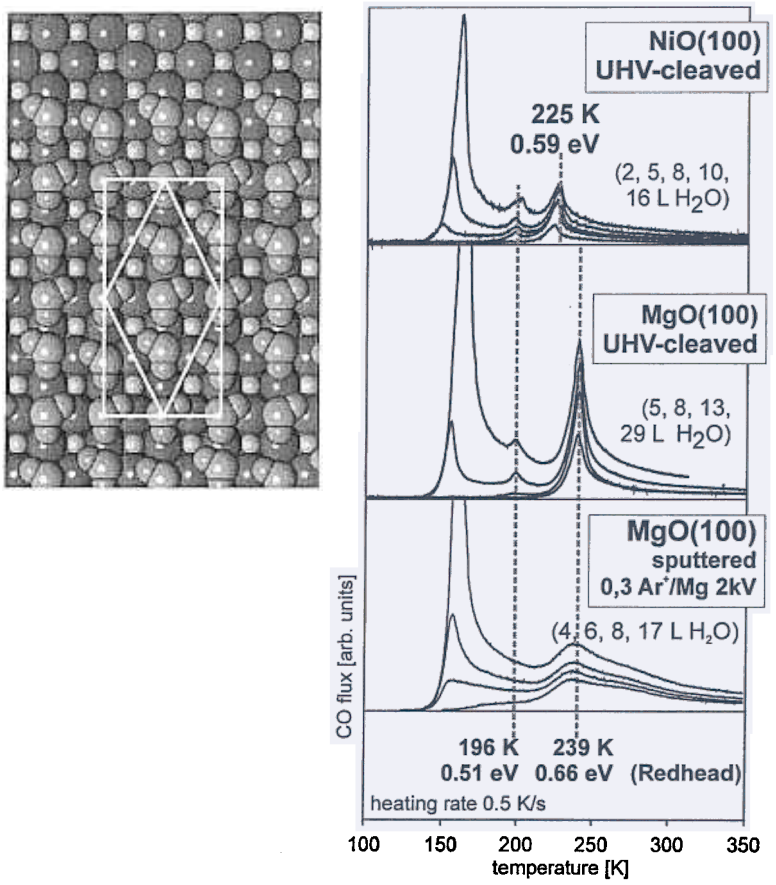

Fig. 12. Thermal desorption spectra of H_2O on UHV-cleaved NiO(100) and MgO(100). A schematic representation of the c(4x2) structure is included (according to ref. [75]). For comparison a thermal desorption spectrum from MgO(100) after creation of defects via sputtering is shown.

sputtering and heating in oxygen. Their TD spectra correspond grossly to the TDS data published by Wichtendahl et al. on in situ cleaved MgO(100) surfaces, which are shown in Fig. 12 [64]. Data taken on a thin MgO film [79] reveal the essential features, although the peaks appear to be shifted significantly with respect to the temperature-calibrated data of Wichtendahl et al. The assignment of the feature at 196 K was unclear so far, although it was near at hand to assume that it is connected with the phase transition from the c(4×2) to the (3×2)pg phase which occurs at about this temperature and was reported by several groups [75, 76, 79]. It could be shown that the molecule density within the c(4×2) phase is higher than in the (3×2)pg phase (~ 1.3 atoms and ~1.0 atoms per magnesium surface ion, respectively) [78] so that a transition between these phases must be accompanied by a desorption peak in TDS. The TDS data of H_2O/MgO(100) in combination with data for H_2O/NiO(100) taken in our group [80] shed new light upon this question. Fig 12 [80] reveals the data. The feature near 150 K is due to multilayer desorption and shall not be discussed here in more detail. The peak at 196 K, which corresponds to the transition from

the c(4×2) phase to the (3×2)pg phase, is observed in the spectra from both surfaces at the same temperature.

This observation is a first hint that part of the molecules of the c(4×2) phase belong to the second layer and do not have contact with the oxide surface. The highest temperature peak, which corresponds to desorption of the (3×2)pg phase in the MgO(100) case, i.e. the monolayer, is found at slightly different temperatures, i.e. 225 K for NiO(100) and 239 K for MgO(100), because the direct interaction between water and the Ni and Mg sites, respectively, is different. This conclusion is supported by results of molecular dynamics simulation by the Besançon group on H_2O/MgO(100) [77]. Results are displayed in Fig. 13 [77]. The interesting result is that a monolayer of H_2O forms with the H_2O molecules oriented with the plane parallel to the oxide surface and with a network of H-bonds within that layer, but fully disconnected from the second and higher layers. This monolayer, which is to be identified with the (3×2)pg phase, completely shields the higher layers from the underlying oxide surface. Therefore, the molecules desorbing during the phase transition from the c(4×2) phase to the (3×2)pg phase may be identified as being part of the second layer, since these molecules do not feel the differences between NiO(100) and MgO(100) as documented by the data shown in Fig. 13.

In closing this chapter we would like to mention that there are several studies in the literature where more complex molecules, which are also of technical interest, have been studied. These include methanol, formic acid and aromatic compounds [81-88]. We shall not dwell on these studies here but merely refer the reader to the literature.

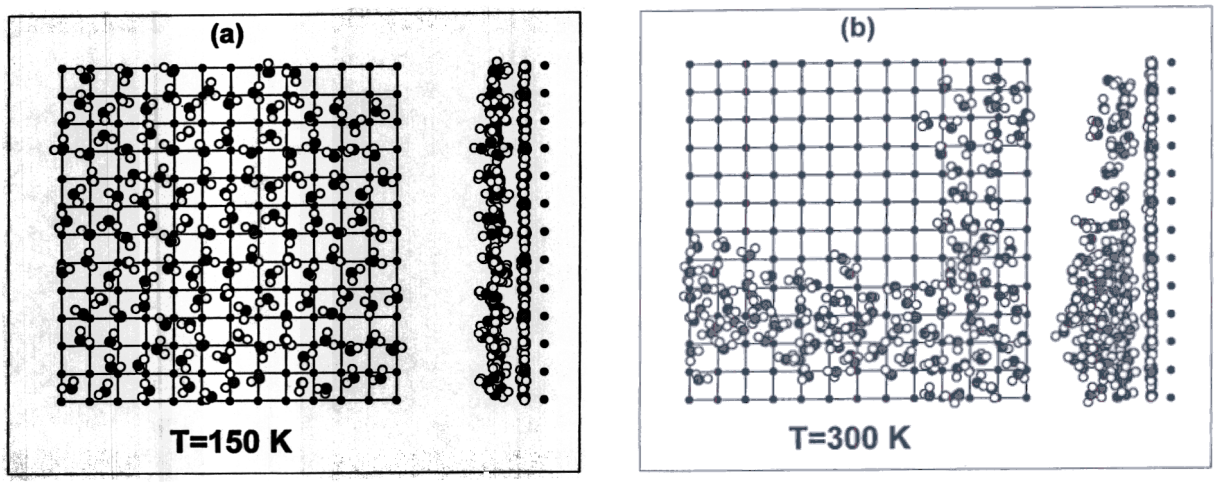

Fig. 13. Simulation of water on MgO(100) at coverages higher than one monolayer at 150 K and 300 K, according to ref. [77]. a) top and side views of map-shots at 150 K. b) top and side views of map-shots at 300 K. (The first layer molecules are not represented in the top view.) The side views show that the overlayer beyond the monolayer tends to aggregate.

3. SURFACES OF OXIDES WITH CORUNDUM STRUCTURE

Fig. 14 shows the lattice structure of a non-magnetic system, i.e. α-alumina [15]. We note here in passing that there are antiferromagnetic corundum structures where the metal centers carry different spin-orientations which renders the size of the unit cell considerably larger [89-91].

The surface energies for a structure as shown in Fig. 14 has been calculated for a variety of orientations [93]. Some of these energies are compiled in Table 3. Surfaces with (0001) and $(11\bar{2}0)$ orientations have been investigated with the large data set available for the (0001) orientation. We therefore restrict ourselves

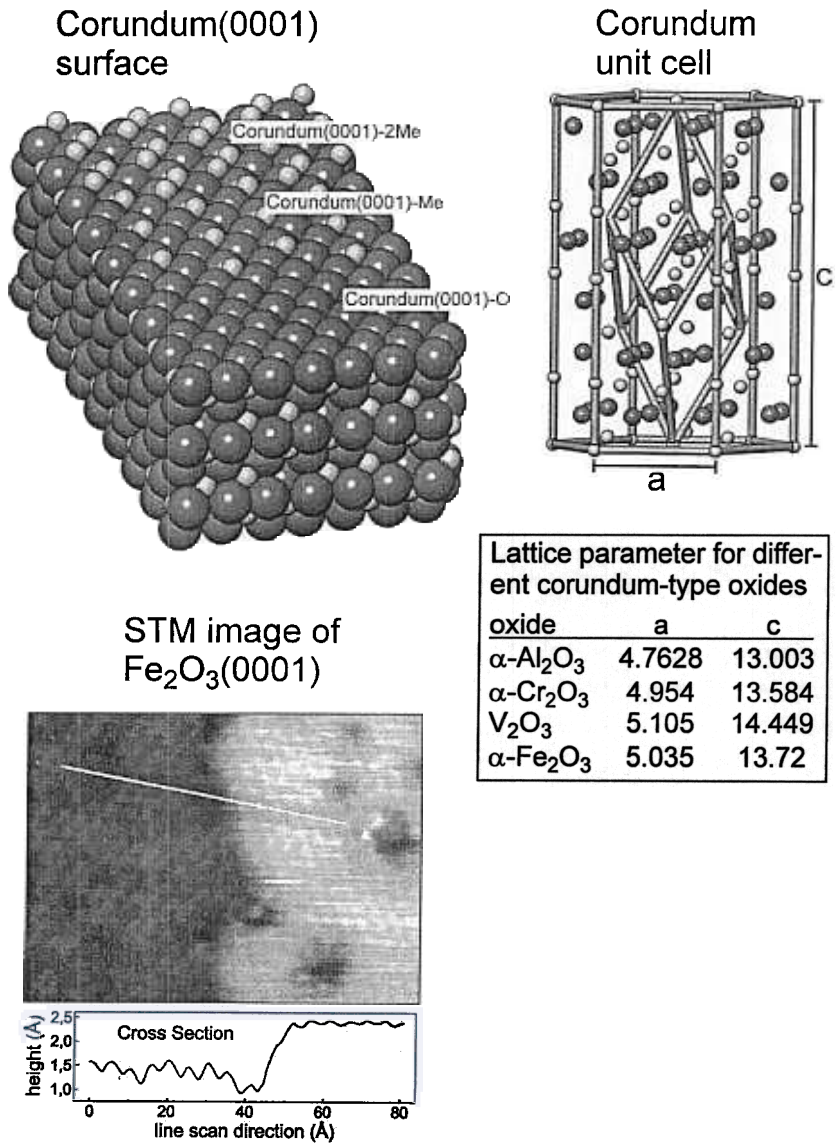

Lattice parameter for different corundum-type oxides

oxide	a	c
α-Al_2O_3	4.7628	13.003
α-Cr_2O_3	4.954	13.584
V_2O_3	5.105	14.449
α-Fe_2O_3	5.035	13.72

Fig. 14. Top: Schematic representation of the corundum unit cell and surface structures with different terminations. Bottom left: Scanning tunneling image of the Fe_2O_3(0001) surface. The darker area is believed to be metal terminated and the brighter area metal terminated according to corundum(0001)-Me [92]. Bottom right: List of lattice parameters for different oxides with corundum structure [15].

Table 3. Recent Surface Energies from First Principles [93]

Surface Orientations	Surface Energy
0001	2.76 Jm^{-2}
$10\bar{1}1$	2.55 Jm^{-2}
$10\bar{1}2$	1.97 Jm^{-2}
$11\bar{2}0$	1.86 Jm^{-2}

to a discussion of the latter case. The (0001) surface is an example for the so-called charge neutralized polar surfaces. These surfaces exhibit relatively strong relaxations remnant of the phenomena discussed in connection with the polar (111) rocksalt type surfaces, because if the (0001) surface were terminated between an oxygen and a metal layer, these surfaces would be polar with a diverging surface potential. However, the surface is terminated with only half of a metal layer present. Formally, this corresponds to a surface created by cutting the bulk structure within the buckled metal ion layers.

Fig. 15 shows the results of structural determinations for the three related systems $Al_2O_3(0001)$ [8], $Cr_2O_3(0001)$ [94, 95] and $Fe_2O_3(0001)$ [96]. In all cases a stable structure in UHV is the metal ion terminated surface retaining only half of the number of metal ions in the surface as discussed above [92]. The interlayer distances are very strongly relaxed down to several layers below the surface [10]. The perturbation of the structure of oxides due to the presence of the surface is considerably more pronounced than in metals, where the interlayer relaxations are typically of the order of a few percent. The absence of the screening charge in a dielectric material such as an oxide contributes to this ef-

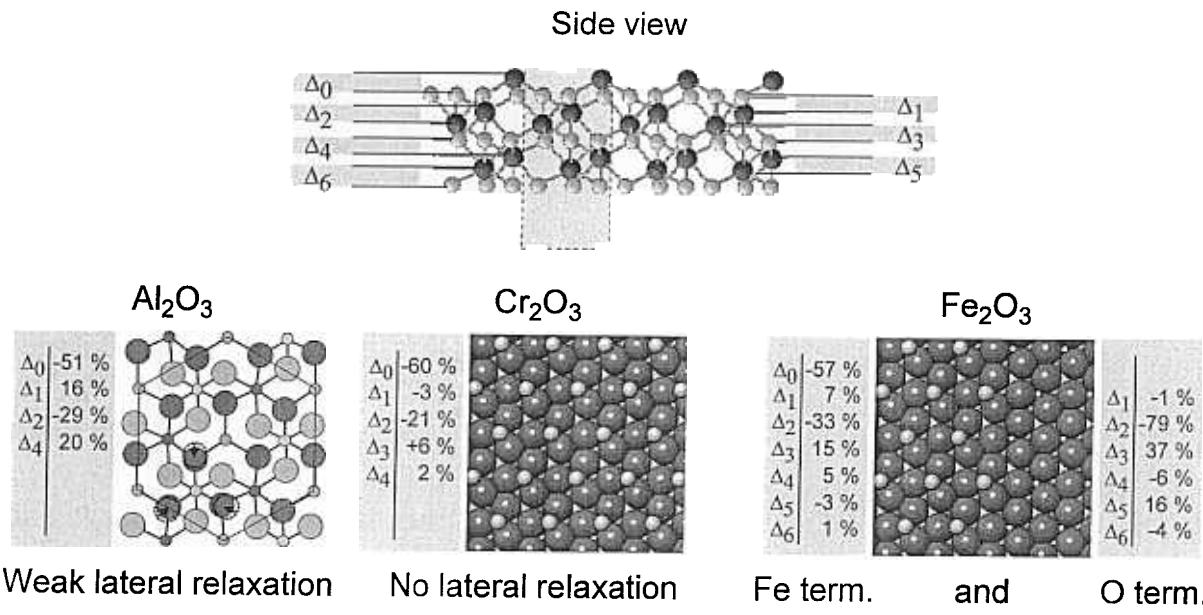

Fig. 15. Experimental data on the structure of corundum type depolarized (0001) surfaces (side and top views).

Fig. 16. Low energy electron diffraction diagram of $V_2O_3(0001)$ grown on Au(111) [98]

fect considerably. Another material belonging to this family is V_2O_3 which can also be prepared as a (0001) surface [97]. The structure of this system has, however, not yet been thoroughly investigated, although the LEED pattern, as shown in Fig. 16, is quite sharp [98]. In this case the V_2O_3 (0001) surface has been prepared as a thin film on a Au(111) substrate by evaporation and oxidation. We assume that the surface structure is similar to the related cases discussed above.

It has recently been pointed out that oxide structures may not be as rigid as one might think judged on the relatively stiff phonon spectrum in the bulk [99, 100]. In fact, at the surface the phonon spectrum may become soft so that the geometric structure becomes rather flexible, and thus also very much dependent on the presence of adsorbed species [100]. The vibration modes of a clean $Cr_2O_3(0001)$ surface have been studied under ultrahigh vacuum conditions with high resolution electron energy loss spectroscopy [100]. Fig. 17 shows the spectrum of the clean surface at the bottom. A mode, which is confined to the first few atomic layers of the oxide, was detected, in addition to the Fuchs-Kliewer phonons, at 21.4 meV. This mode shows only a very small isotopic shift when the $Cr_2O_3(0001)$ film is prepared from $^{18}O_2$ instead of $^{16}O_2$. In contrast to the Fuchs-Kliewer phonons which extend deeply into the bulk the 21.4 meV mode is very sensitive towards the presence of adsorbates, as is shown in Fig. 17. This can be seen by its attenuation upon exposure of the surface to CO, which in this case is only weakly adsorbed. Full-potential linearized augmented plane wave calculations [100] show that this mode is an in-phase oscillation of the second-layer oxygen atoms and the Cr atoms of the two layers below. A schematic representation of the mode is shown in the inset of Fig. 17.

Bulk oxide stoichiometries depend strongly on oxygen pressure, a fact that has been recognized for a long time and we have alluded to above [10]. So do oxide surfaces, structures and stoichiometries, a fact that has been shown again in a recent study on the $Fe_2O_3(0001)$ surface by the Scheffler and Schlögl

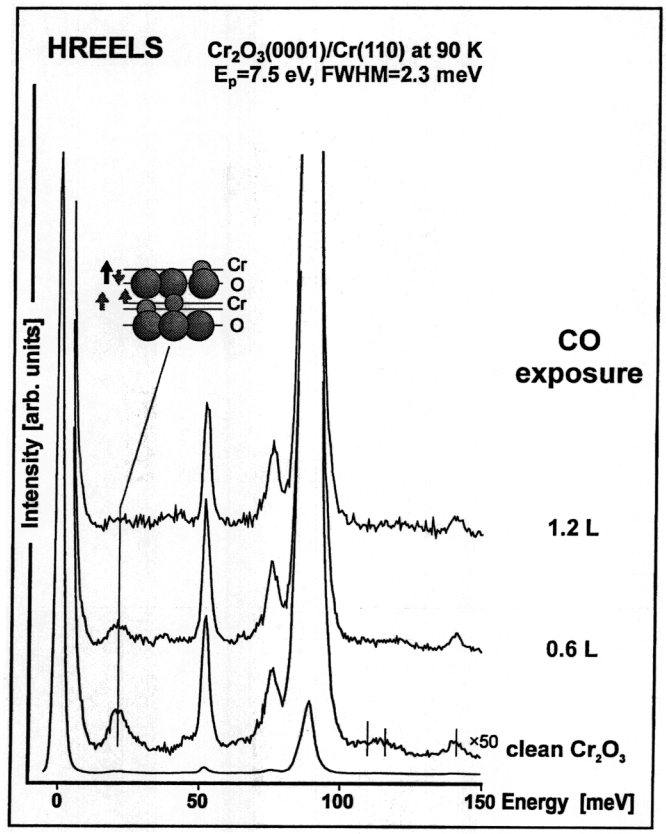

Fig. 17. Electron energy loss spectra in the vibrational regime of clean and CO-covered Cr_2O_3(0001)/Cr(110) surface. (E_p: 7.5 eV, specular scattering) The inset shows a schematic representation of the calculated normal mode of a Cr_2O_3(0001) surface at 21.4 meV, according to ref. [100].

groups [92]. In fact, if a Fe_2O_3 single crystalline film is grown in low oxygen pressure, the surface is metal terminated while growth under higher oxygen pressures leads to oxygen termination. This surface would be formally unstable on the basis of electrostatic arguments [10]. However, calculations by the Scheffler group have shown that a strong rearrangement of the electron distribution as well as relaxation between the layers leads to a stabilization of the system. STM images by Weiss and co-workers corroborate the coexistence of oxygen and iron terminated layers and thus indicate that stabilization must occur. Of course, there is need for further structural characterization. For the surface of Cr_2O_3(0001) infrared spectroscopic data suggest a different termination when the clean surface is exposed to oxygen [101] as will be discussed below.

The electronic structure of corundum type oxide surfaces have been studied with photoelectron spectroscopy [102, 103] as well as with electron energy loss spectroscopy [104]. Henderson and Chambers [103] have recently reviewed the photoelectron spectroscopic evidences. Still, there seems to be an ambiguity about the oxidation state of the chromium ions in the immediate surface layer. XPS Cr 2p data may be to a large extent reconciled as being due to Cr(III) in the surface, because there is obviously no change in the spectra as a function of

emission angle. However, cluster calculations indicate that even though the number of d-electrons on the Cr ions is compatible with Cr^{3+}, the total charge on the Cr ions is closer to Cr^{2+} because of a considerable hybridization between the chromium and oxygen wave functions [104]. In a previous review we have discussed the assignment of the local d-excitations on chromia surfaces and the reader is referred to this paper for details [7]. We would like to mention, however, a particular aspect of surface charge transfer excitations for the case of chromia(0001) which also touches upon the question of the oxidation state of surface chromium ions. The charge transfer states often mark the edges of the band gap in transition metal oxides, and they are also modified by the presence of the surface. Unfortunately, NiO does not show this effect very clearly. The electronic excitations at the chromia(0001) surface, on the other hand, are good examples to discuss the phenomenon.

Fig. 18 shows the EELS spectrum [105-107] of this surface at low temperature. Again, a thin film has been used. The sharp features in the band gap are excitations within the manifold of d-orbitals. A detailed discussion [107] has shown that the excitations are characteristic of surface Cr ions with three d-electrons. However, the Cr ions do not carry a net charge of 3+ as expected (and found for the bulk Cr ions) but rather of 2+ charge due to strong hybridization with the neighboring oxygen atoms. When we now perform EELS measurements after adsorption of CO_2, not only the d-excitations are influenced but also the very intense feature near 4.8 eV. Again, on the basis of cluster calculations performed in the Staemmler group [104], it has been possible to assign this intense feature to a surface charge-transfer excitation at the band gap, which is shifted to lower energy as compared with the corresponding excitation in the bulk (see Fig. 18). The decrease in energy is reasonable because the Cr d-orbi-

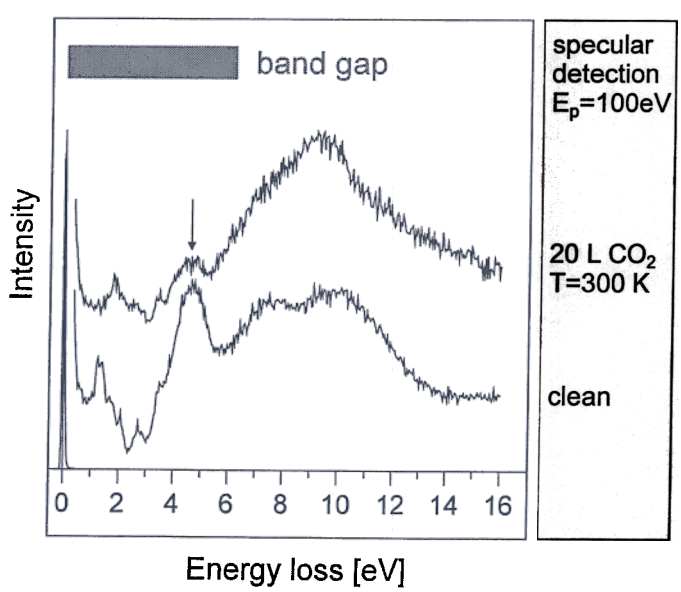

Fig. 18. EELS spectra of the clean and adsorbate covered Cr_2O_3(0001) surface. Peak assignments are indicated [105-107].

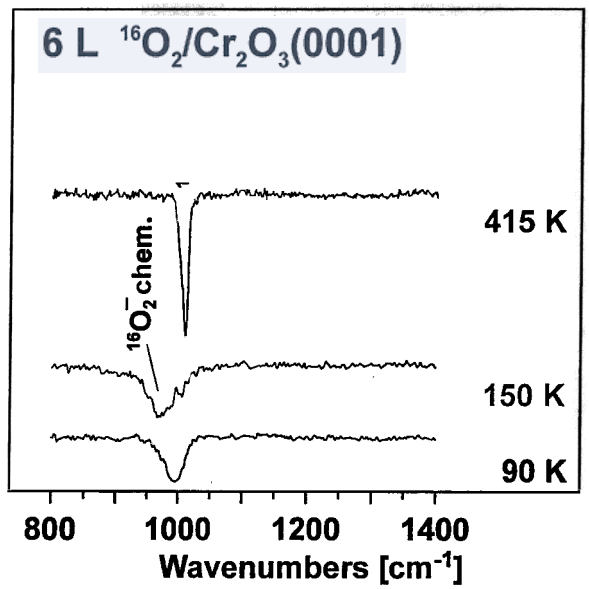

Fig. 19. IRAS spectra after adsorption of a saturation coverage of O_2 on $Cr_2O_3(0001)/Cr(110)$. The spectrum at the bottom was taken at 90 K. Other spectra are taken at the temperatures indicated [101].

tals have been lowered, the more open surface structure (see Fig. 15) and the coordination of the Cr ions to only three oxygen ions allows for better charge separation than in the bulk. In NiO the effect is less pronounced because the surface Ni ions are still five-fold coordinated.

The analysis of the electronic structure of $Cr_2O_3(0001)$, as discussed so far, has been performed at 90 K. We note that upon increasing the temperature, the structure of the surface changes [107], and we have speculated that these changes are connected with changes in the magnetic structure of the surface. Oxide surface magnetism is a field that needs to be explored in the future.

Before we discuss the adsorption and bonding of molecules such as CO and NO to the corundum type surfaces in order to accentuate the differences with respect to the rocksalt type surfaces, we would like to comment on the chemistry of molecular oxygen on the corundum type surfaces. As the (0001) corundum type surfaces are depolarized polar surfaces we always have to define whether we are talking about the metal terminated or the oxygen terminated surface. If not mentioned specifically we always assume metal termination. Chromia when exposed to oxygen leads to a very interesting chromyl terminated surface. What do we know about the chemistry between molecular oxygen and chromia(0001) that leads to this final result? Figure 19 shows the appearance of a sharp line in infrared spectra which develops out of a broad feature after heating the surface to room temperature. As has been discussed earlier and also supported by isotopic labeling experiments by Dillmann et al. [101] chromyl groups are formed on the surface and it was suggested that the chromium ions in the surface layer of the clean surface bind oxygen to form such chromium-oxygen double bonds. As is obvious from Fig. 19 there are adsorbed oxygen precursors to the chromyl

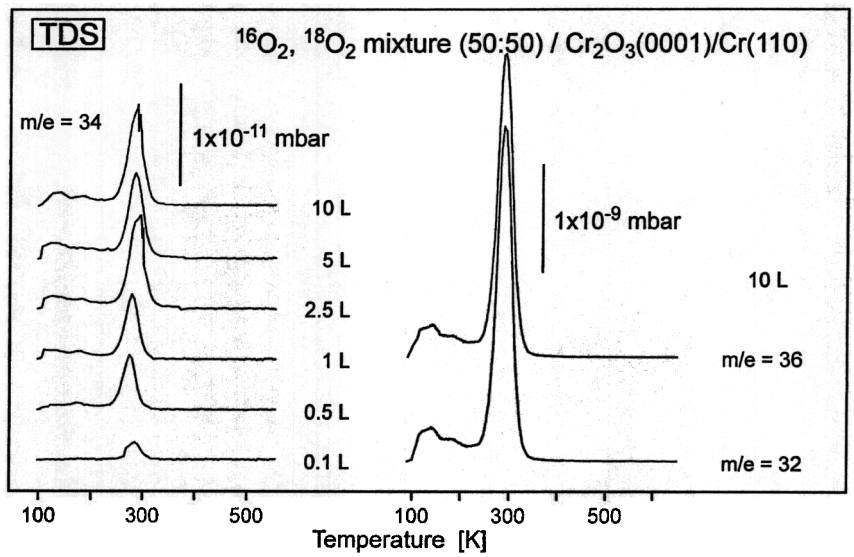

Fig. 20. Thermal desorption spectra of oxygen desorbing from Cr_2O_3(0001) [101].

formation. The width as well as frequency is indicative of a O_2^- species being adsorbed on the surface in a more or less upright position [101].

Fig. 20 is indicative of the thermal chemistry going on the surface. The TDS data reveal that around room temperature most molecular oxygen is lost from the surface. This molecular oxygen does not result from a recombinative desorption as can be seen directly from the isotopic labeling experiments. There is basically no isotopic mixing beyond the originally present contaminants. Above room temperature there is a very high temperature peak due to recombinative desorption stemming in all likelihood from the chromyl oxygen present on the surface at elevated temperatures, and observed in the infrared spectra. We will see further below examples of how these chromyl groups influence the chemistry of other adsorbed species on the surface.

CO adsorption on corundum type (0001) surfaces is interesting because, opposite to checker board rocksalt type surfaces, on the (0001) surface of Cr_2O_3 CO has been shown by angle resolved photoemission to assume a strongly inclined almost flat adsorption geometry. Infrared spectroscopy and recent cluster calculations by Staemmler's group have revealed the reason for this [108]. Briefly, on the basis of TDS data the activation energy for the desorption of CO from chromia(0001) is estimated to be about 45 kJ/mol. So the appropriate state may be termed weakly chemisorbed. In addition, more weakly bound CO molecules (28 kJ/mole) which are present on the surface at lower temperature have been detected. Multilayer adsorption of CO does not occur on Cr_2O_3(0001)/Cr(110) at 90 K. IR-spectra confirm the presence of different CO species on Cr_2O_3(0001). Fig. 21 shows a series of IRAS-spectra as a function of initial CO dosage at 90 K. Using a CO-exposure of 0.05 L we detect a signal of the CO-stretching vibration at 2178 cm^{-1} and at 0.1 L a second signal appears at 2165 cm^{-1}. With increasing coverage the high-frequency signal considerably

increases and slightly shifts to lower wave numbers. The weak signal at 2165 cm^{-1} does not gain further intensity. Instead it disappears in the shoulder of the main signal. This state is to be correlated with the chemisorbed state observed in TDS. Finally, at exposures above 3 L a third signal appears at 2136 cm^{-1}, which is due to the more weakly held species.

Cluster calculations and TDS measurements agree fairly well as far as the adsorption of CO at the $Cr_2O_3(0001)$ surface at low coverages is concerned. The chemisorbed species corresponds to an undissociated CO molecule residing in the O_3-hollow position with the CO axis strongly tilted against the surface normal, oriented along a line connecting two surface Cr ions and in a hollow position with respect to the O^{2-} ions in the second layer. The more weakly held species corresponds to a shallow local minimum in the potential energy curve, in which CO lies nearly flat on the surface, also between two surface Cr ions, but on top an O^{2-} in the second layer (O-ontop position).

In contrast to the adsorption geometry there is some discrepancy concerning the adsorption energies as calculated by the cluster calculations. The values of 45 and 28 kJ/mol estimated for the two TDS peaks from the Redhead formula are considerably larger than the calculated values of about 27 and 15 kJ/mol. As has been pointed out in connection with NiO, it has to be expected that the calculated values are too low since neither adsorbate-induced relaxations of the

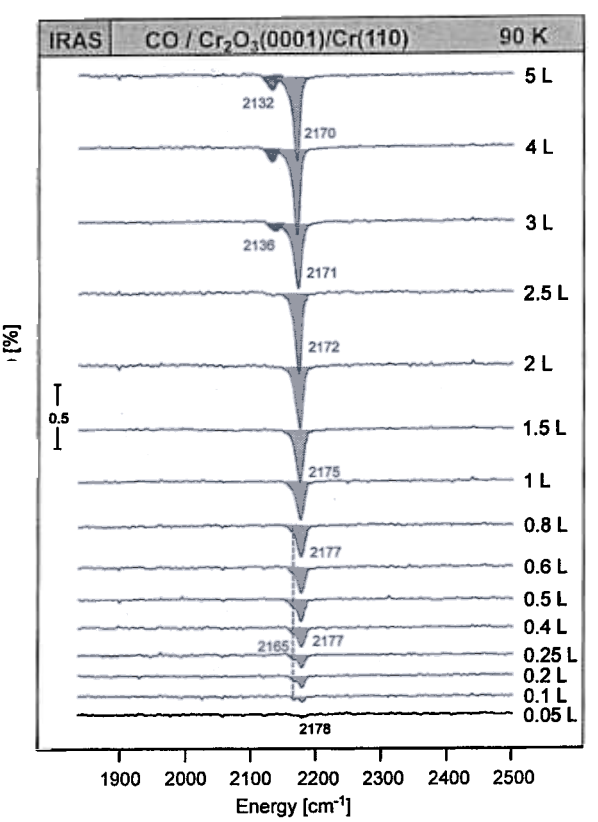

Fig. 21. FTIR spectra of CO adsorbed on $Cr_2O_3(0001)$ at 90 K as a function of exposure [108].

$Cr_2O_3(0001)$ surface nor extra cluster van der Waals attractions are accounted for. Whether the inclusion of these effects will lead to a perfect agreement with the measured values is not clear. In any case it seems justified to call the O_3-hollow minimum a „chemisorption" though the dominant contribution to the interaction energy has electrostatic origin and is characterized by the situation in which the quadrupole moment of CO fits into the strongly inhomogeneous electrostatic field above the $Cr_2O_3(0001)$ surface.

Good agreement between theory and experiment exists concerning the frequencies shifts of the CO stretching vibration. The calculations predict a blue shift of about +22 cm^{-1} for the CO in the O_3-hollow position, which compares favorably with the observed shift of 30-35 cm^{-1} in the most prominent IRAS band. For the weakly bound CO in the O-ontop position a small red shift of about –5 cm^{-1} is obtained; the signal at 2136 cm^{-1} observed at higher coverages for the weakly bound CO species does indeed exhibit such a small red shift of -7 cm^{-1}. However, the ab-initio calculations cannot offer an explanation for the shoulder in the IRAS peak at 2165 cm^{-1} observed for dosages in the range between 0.1 and 0.8 L (Fig. 21). The frequency itself seems to correspond to that of CO in the Cr-ontop position, but this does not constitute a local minimum and will hence be not occupied. We also might speculate that the shift observed in the main IRAS peak from 2178 cm^{-1} at low coverage to 2170 cm^{-1} at high coverage is due to lateral CO interactions, most probably because each CO molecule is slightly squeezed out of the absolute minimum by neighboring CO molecules.

The results of the present study should also be interrelated with UPS and NEXAFS experiments which have been performed on the $CO/Cr_2O_3(0001)/Cr(110)$ system previously [105, 106]. Whereas the present data allow the identification of strongly and weakly bound CO molecules, only the more strongly adsorbed species has been observed in the photoelectron spectroscopic studies. The explanation may be found in the experimental conditions: At the slightly elevated surface temperature (105 K) used in those experiments and because of UV- and X-ray-induced CO-desorption the weakly bound CO species could not be detected. (In fact, the UPS and NEXAFS measurements had to be performed at a background CO pressure of 1×10^{-8} mbar.) A very interesting point is the adsorption geometry of the CO-species on $Cr_2O_3(0001)/Cr(110)$. On the basis of the ARUPS and NEXAFS data [105, 106] the tilt angle between surface plane and molecular axis of the chemisorbed CO was estimated to be about 20°. The present IR-data are consistent with an adsorption model of a strongly tilted CO-chemisorbate, in line with the cluster calculations.

On the other hand, the IR-signal of the weakly bound CO-species (at ≈ 2136 cm^{-1}) shows a very small intensity compared to the relative population of states as deduced from TDS (not shown) [108]. Neglecting possible differences in the strength of the dynamic dipoles we can conclude that for the

weakly bound CO molecules the tilt angle between surface normal and molecular axis is even larger than for the chemisorbed CO: the weakly bound CO lies almost flat on the surface. This conclusion is confirmed by the cluster calculation as well.

It is very interesting to note that CO adsorption on $V_2O_3(0001)$ seems to show a very much related behavior although the study of orientation of the molecule is not complete yet [98].

Water adsorption has been studied for Fe_2O_3 as well as for $Cr_2O_3(0001)$ surfaces by Henderson and Chambers [103, 109, 110]. In general, both, dissociative adsorption as well as molecular water adsorption has been observed. Fig. 22 shows TDS data for chromia [103]. The low temperature peak corresponds to molecular physisorption, including multilayer formation (peak at 165 K), while the higher temperature peaks are consistent with, partially, recombinative desorption of chemisorbed water from the surface. The two states at 295 K and at 345 K are populated sequentially, starting with the high temperature state at the lowest exposure. Vibrational spectra revealed the presence of isolated hydroxyl groups. These are associated with the peak at 345 K. In fact, Henderson and Chambers [103] proposed that water in the dissociated state is comprised of two distinct hydroxyl groups, i.e. a terminal and a bridging hydroxyl group. Molecularly chemisorbed water desorbs at 295 K. These authors also mention the strong influence of a predosage of the surface by oxygen on the surface

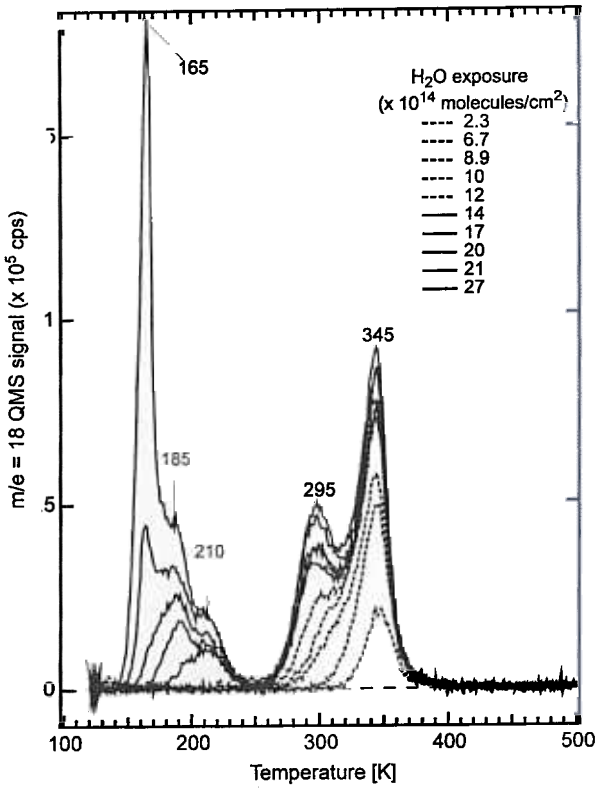

Fig. 22. Thermal desorption spectra of water desorbing from $Cr_2O_3(0001)$ after various exposures [103].

chemistry. Their observations are in line with results on the adsorption of CO_2 described briefly below [111, 112].

Water adsorption on alumina leads to molecular adsorbates [110]. There are some reports on the formation of isolated hydroxyl groups on regular sites [113, 114]. Whether they are the results of dissociative water adsorption is not completely clear, although there is a recent theoretical paper that predicts the dissociation of water on $Al_2O_3(0001)$ by protonation of a surface oxygen, while the molecule previous to dissociation resides on a cation site [115]. There is no experimental verification of this result as yet. There are, however, explored routes to hydroxylate alumina surfaces either by exposure to atomic hydrogen or by a combination of aluminium deposition and subsequent hydrolyzation with water [116].

Carbondioxide adsorption is another example of molecular adsorption which has been studied quite extensively in the past. While for some time is was generally accepted that CO_2 forms carbonates with chromia surfaces very readily upon exposure, it was recently observed that carboxylate species may be formed. TDS spectra indicate [111, 112] that there are more weakly and less weakly bound CO_2 species on the surfaces. We have studied the nature of those species by various techniques including infrared spectroscopy. Fig. 23 shows several sets of IR spectra. The pair of sharp bands around 2300 cm^{-1} can easily be assigned to the more weakly bound CO_2 with only slightly distorted structure

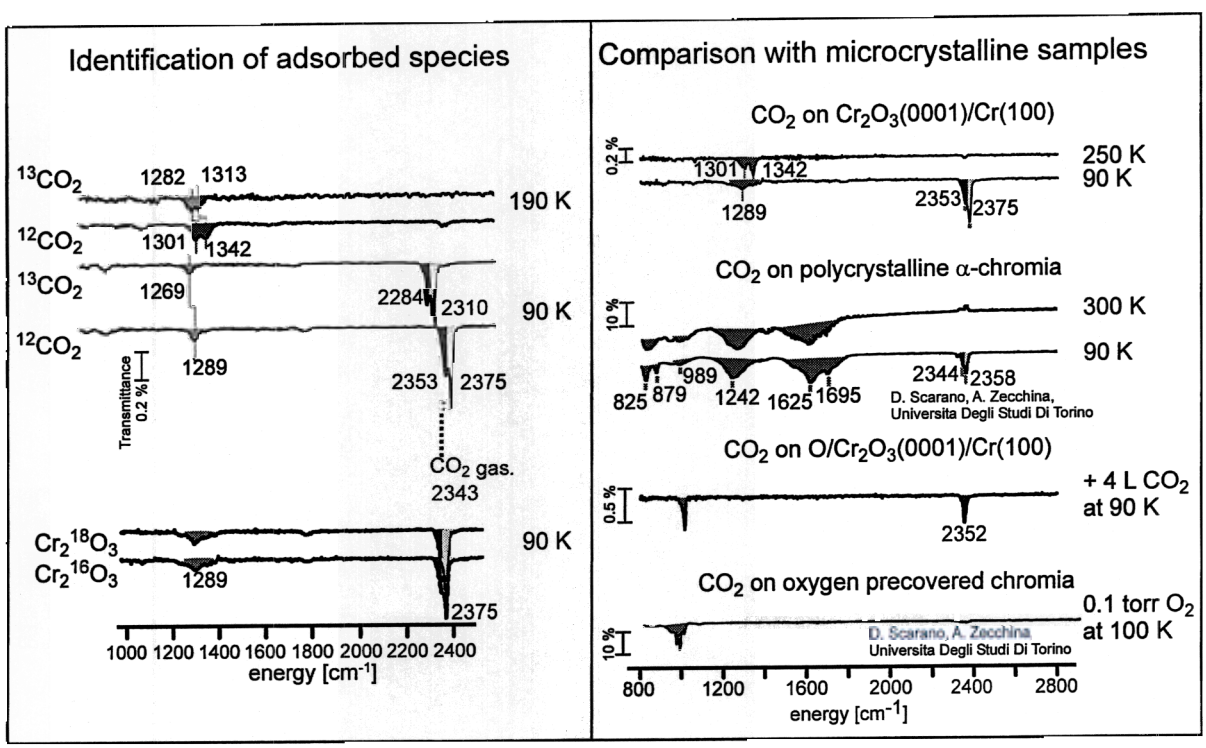

Fig. 23. IRAS spectra of CO_2 adsorbed on $Cr_2O_3(0001)$ surfaces and on polycrystalline chromia, left panel: IRAS spectra at different surface temperatures and with isotopically labeled CO_2 as well as Cr_2O_3, right panel: adsorption of CO_2 after pre-adsorption of oxygen [112].

as compared with the gas phase species. By a combination of isotopic labeling the adsorbed CO_2 (shift of frequencies) as well as the oxide layer (no shift of CO_2 bands) we have demonstrated that the single band centered around 1300 cm^{-1} is due to the presence of a carboxylate species, i.e. a bent anionic CO_2 species, and not, as perhaps expected, to a carbonate [105].

The bands between 1610 and 1700 cm^{-1} are missing because of the applicability of surface selection rules in thin film systems. This means, all non-totally symmetric bands are suppressed in intensity. A quick comparison with CO_2 adsorption on chromia microcrystalline material as shown in Fig. 23 indicates the presence of the bands between 1610 and 1700 cm^{-1} as expected for adsorption on a bulk dielectric material. It is remarkable how similar the thin film data are in comparison with the microcrystalline material. This has been discussed in detail by Adriano Zecchina's group [117]. Also, the response of the two systems with respect to preadsorption of oxygen is very similar. In fact, as shown in Fig. 23, CO_2 adsorption in form of the less weakly bound CO_2^- is fully suppressed on the thin film system and very strongly attenuated for the microcrystalline system. This indicates that CO_2 occupies the chromium sites, because we know that oxygen from the gas phase adsorbs on the chromium ions. As we remarked above, ELS [106] and XPS [102] spectra of the $Cr_2O_3(0001)$ surface have been used to deduce that the Cr-ions in the surface are in a low oxidation state, i.e. Cr^{2+} as opposed to chromium ions in the near surface and bulk regions. It is therefore not surprising that such a surface provides electrons to adsorbed molecules, leading to electron transfer as, for example, documented by the formation of O_2^- and CO_2^-. The low valence state of the Cr surface ions also has consequences in other reactions, such as the polymerization of ethene which has been studied on $Cr_2O_3(0001)$ [118], and in connection with other model studies [119].

A tri-atomic molecule that has so far not found wide attention is NO_2, although the molecule is interesting with respect to environmental catalysis [120]. We have studied the interaction of NO_2 with alumina films [121]. Fig. 24 shows TDS data for this system: The dosages given in Fig. 24 are expressed in terms of the rise of the base pressure for 10 s at a fixed distance between doser and surface. By multimass TPD measurements it has been checked that NO_2 is the only desorbing species. For small coverages a single desorption peak is found at 135 K which saturates at higher exposures. This first desorption peak can be assigned to isolated NO_2 molecules physisorbed to the oxide with a binding energy of 38 kJ/mol estimated according to Redhead's analysis [65]. At higher coverages a second desorption feature at nearly 10 K higher temperature appears. The observation of a TPD peak at higher temperature which does not saturate upon increase of exposure is quite unusual compared to the "normal" desorption behavior of, e.g., NO_2/Au(111) published by Bartram and Koel [122]. It indicates an intermolecular interaction energy larger than the binding energy from the

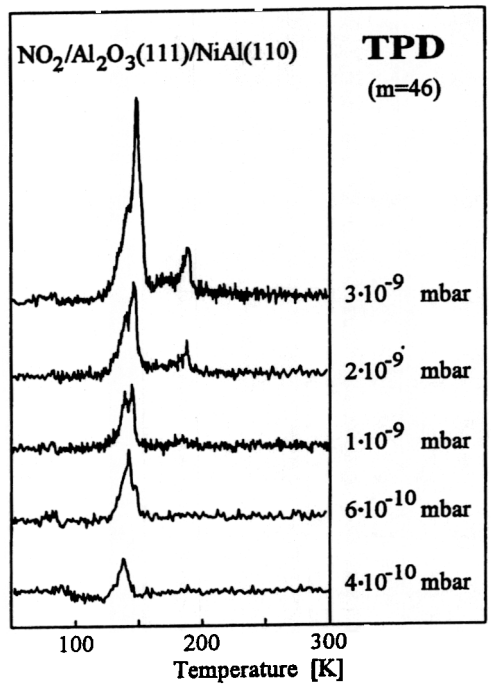

Fig. 24. Thermal desorption spectra of NO_2 desorbing from Al_2O_3 after exposure to various background pressures at 50 K.

molecule to the substrate. This desorption with higher binding energy may be due to two- and three-dimensional molecular aggregates, respectively.

Obviously, there is not a strong interaction of the molecule with the substrate rendering the surface chemistry in this system rather simple. However, due to the radical nature of NO_2 this system offers unique possibilities to study molecular motion of adsorbed molecules by applying electron spin resonance (ESR) spectroscopy under UHV conditions [121, 123]. We have developed this technique to be applied under UHV conditions to the systems addressed here and we refer the reader to the literature for technical details of the experiment [123]. Since ESR spectroscopy is a widely applied technique in chemistry we assume that the reader is familiar with the general ideas of ESR spectroscopy, although we realize that in the surface science community this may not be the case [124]. Fig. 25 shows ESR spectra for the system NO_2/Al_2O_3. Before we go into details of the spectra in Fig. 25 we try to explain the characteristics of the recorded ESR spectra. There are two main contributions to the habit of the spectra. First, the unpaired electron resides in a particular electron orbital of the molecule with a specific spatial orientation, which in turn leads to a dependence of the electron spin resonance on the orientation of the molecule in the external magnetic field. In other words, the isotropic g value of the free electron is transformed into an anisotropic g tensor, which gives rise to a splitting of the resonance lines. The hyperfine interaction of the unpaired electron with the nuclear spin (I = 1) of the nitrogen atom (^{14}N) as the second contribution may be described by the A tensor and finally leads to an appearance of the spectrum, ex-

hibiting three well-separated parts. The spectra are presented as the first derivative of the microwave absorption as a function of the external field.

In Fig. 25 coverage dependent ESR spectra of NO_2 on $Al_2O_3(111)$ are shown. The main observation is the increasing line width ΔB of the spectra with increasing coverage. Assuming the line width to be due to dipolar interaction ($\Delta B \sim 1/r^3$) of the unpaired spins of neighboring molecules [125], it is obvious from the increase of the line width that the distance of the NO_2 molecules decreases. If the sample is annealed at different temperatures, as shown in the lowest spectrum in Fig. 25 and in the inset, a drastic decrease of line width and intensity after annealing to temperatures above 60 K is observed, although temperatures are well below the desorption temperature of 135 K. At about 100 K the decrease of intensity causes the spectrum to vanish below the detection limit within a few minutes.

The decreasing of the concentration of NO_2 is caused by the reaction of paramagnetic NO_2 monomers to the diamagnetic N_2O_4 dimer [126]. Because at low temperatures the equilibrium of this reaction completely favors the dimer, there must be a kinetic restriction causing the molecule not to dimerize at low tem-

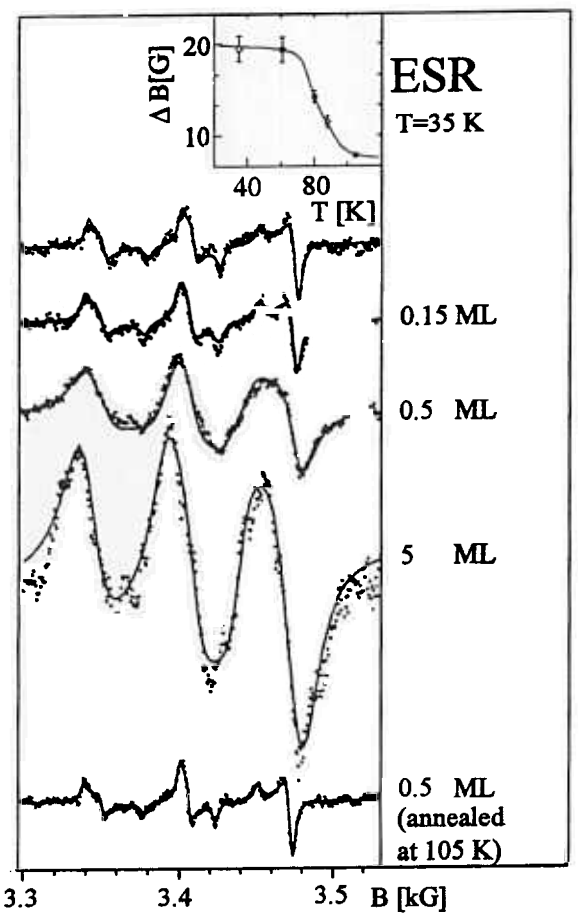

Fig. 25. Electron spin resonance spectra of NO_2/Al_2O_3 adsorbates at different NO_2 coverages. The bottom trace was recorded after 0.5 ML coverage had been annealed at 105 K. The inset shows the line widths as a function of temperature [121].

peratures. We believe the onset of the reaction is coincident with the onset of translational diffusion of the NO_2 monomers on the surface. If the annealing procedure is repeated or continued over larger time intervals the decrease of the line width stops at a certain value (see the inset in Fig. 25), but the signal intensities continue to decrease below the limit of noise. At very low coverages no decrease of the line width can be observed, because it has reached its lower limiting value even after adsorption. This value may be assumed when intermolecular distances between the monomers become so large that the contribution of the dipolar interaction to the line width can be considered to be small as compared to other contributions. Then the only effect of the dimerization process is decreasing the spectral intensity. We compare computer simulations with the spectra in Fig. 25. The model for fitting these spectra is a three-dimensional random distribution of static molecules yielding a so-called powder pattern. A detailed description of the fitting procedure is given in [127, 128]. The simulations match the experimental spectra except for some small differences.

ESR spectra of a submonolayer coverage of NO_2 were taken at different temperatures by warming the sample up step by step before recording the spectra. As mentioned above the signal intensity decreases within a few minutes at about 100 K, rendering it impossible to obtain spectra with a reasonable signal-to-noise ratio. However, it is possible to deduce an estimate for the diffusion coefficient D from this time behavior. Assuming the dimerization to be a diffusion controlled reaction, the theoretical investigation of Freemann and Doll [129] provides a relation between the rate constant observed and the diffusion coefficient. An evaluation in this framework yields a value of $D \sim 10^{-15}$ cm^2/s. The estimates based on coverage and spectral intensity versus time are quite crude; however, the calculated diffusion coefficient is remarkably small, compared to those measured, for example, for CO/Ni(100) [130] ($10^{-5} - 10^{-7}$ cm^2/s).

The analysis so far has been restricted to translational motion. While the detailed analysis of the spectra, in particular at low temperature, also reveal details of the other aspects of molecular dynamics, i.e. rotational motion, the low temperature onset of dimerization in the case of NO_2 obscures this to some extent [131]. It is therefore favorable to investigate radicals which do not dimerize. A typical example is the molecule DTBN (di-tert-butyl nitroxide) which represents basically an NO molecule carrying two bulky hydrocarbon side chains at the nitrogen end which keeps it sterically from dimerizing (see inset in Fig. 26).

The adsorption behavior of this species is relatively complex and has been discussed in detail elsewhere. Briefly, there are three different binding modes of the molecule to the surface, only one of which is ESR active, i.e. still carrying an unpaired electron. The dynamics of this species, which represents about 10% of a monolayer, has been studied with ESR. The molecule is bound to an aluminium cation site via the oxygen lone pair and resides in an environment es-

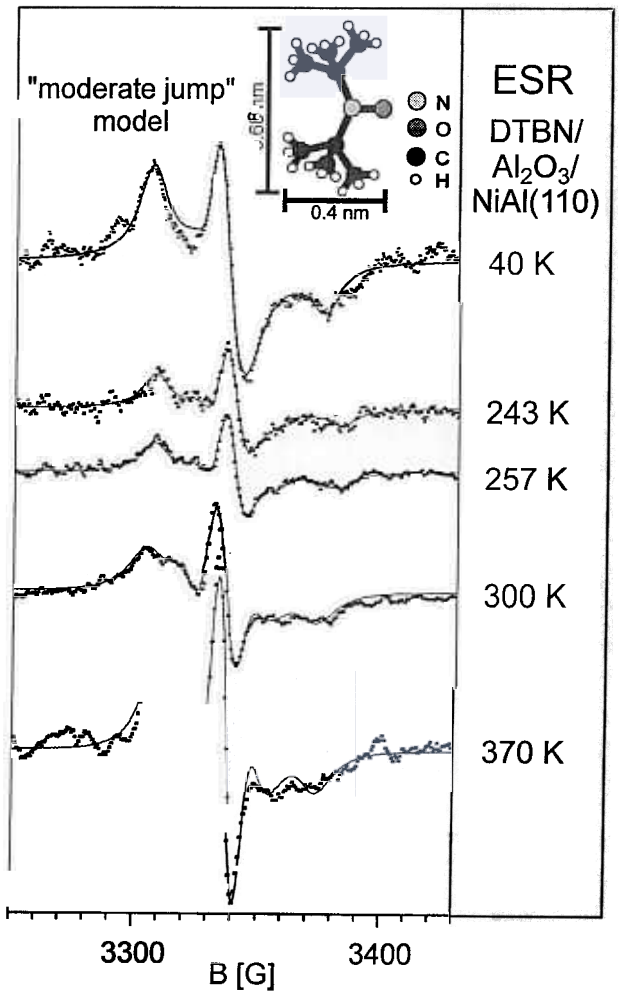

Fig. 26. Electron spin resonance spectra of a DTBN (structure see inset) adsorbate at various temperatures [131].

tablished by a large fraction of molecules bound with both nitrogen and oxygen end to the surface, being however, non ESR active. Therefore the ESR active molecules are well diluted on the surface and exhibit well resolved ESR line shapes as shown in Fig. 26. Here the temperature dependence of the species has been recorded. Below 200 K a rigid-limit ESR spectrum as shown in Fig. 26 is obtained at 40 K. The parameters gained from this spectrum (g and A tensor components) form the basis for the simulation of spectra measured at higher temperature including the effects of molecular dynamics.

Above 200 K changes in line shape as shown in Fig. 26 reveal the onset of molecular dynamics (the simulations (solid lines) are carried out assuming a particular motional model, the "moderate jump" model, which is discussed below.) The line width has dropped to about 12 G, which is known to result from intramolecular interactions manifested as unresolved proton hyperfine splittings [132]. The dipolar interactions are now averaged out by the molecular dynamics. The remarkable intensity behavior (increasing intensity at higher tem-

perature) is caused by the reversible conversion of DTBN molecules from the ESR-inactive to the ESR-active state and is discussed elsewhere [133].

Four different models for the molecular dynamics have been tested to simulate the experimental spectra. Brownian rotational diffusion and jump type diffusion [134, 135] have been used for this analysis, both in their pure forms and in two mixed models. Brownian rotational diffusion is characterized by the rotational diffusion constant D and jump type motion by a residence time τ. The motions have been assumed to be isotropic. In the "moderate jump" model [135], both Brownian and jump type contributions to the motion are coupled via the condition $D\tau = 1$.

The dynamics of the adsorbed DTBN molecules have two components: first, the jump contribution, which may be taken to represent the fast switching between the six equivalent positions around an aluminum binding center at the surface as shown in Fig. 27; second, an additional tumbling contribution which cannot be caused from collisions with gas phase molecules, since the experiment takes place under UHV conditions. The high stability of the adsorbate under UHV conditions also rules out a translational diffusion of the DTBN molecules. The tumbling involves two other motional degrees of freedom for the DTBN molecule as a whole: a rotation around the binding axis and a vibration against the surface. If both motions are of low amplitude, they may be reflected in the additional Brownian contribution to the jumping motion. The low-amplitude tumbling is traceable to the bulky tert-butyl groups which interact via van der Waals forces with the surface and restrict both movements to small angles. The rotation around the binding axis can also be identified as illustrated in Fig. 27. The vibration of the molecule against the surface can be seen as a hindered rotation of the molecule around the aluminium center as also shown in Fig. 27.

ESR spectroscopy has also been used to study dynamics in more complex systems on oxide surfaces, i.e. self-assembled molecular (SAM) films [136, 137]. Fig. 28 shows ESR spectra taken for spin labeled stearic acid, namely n-doxyl-stearic acid (n-DXSA) immersed onto a thin alumina film. These nitroxides, with an oxazolidinyl ring as paramagnetic group connected to different po-

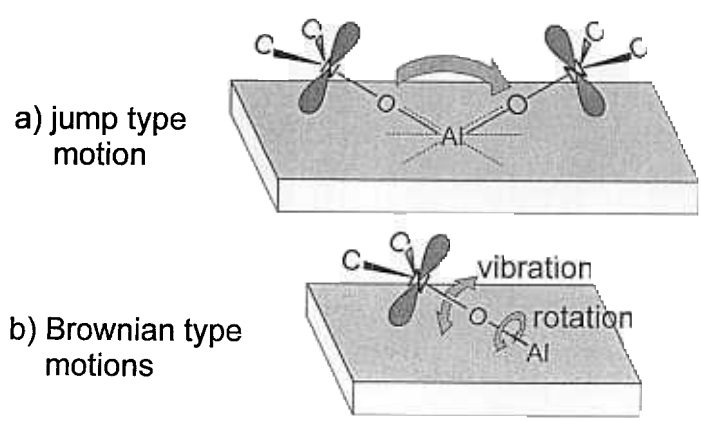

Fig. 27. Schematic representation of motions of DTBN on Al_2O_3

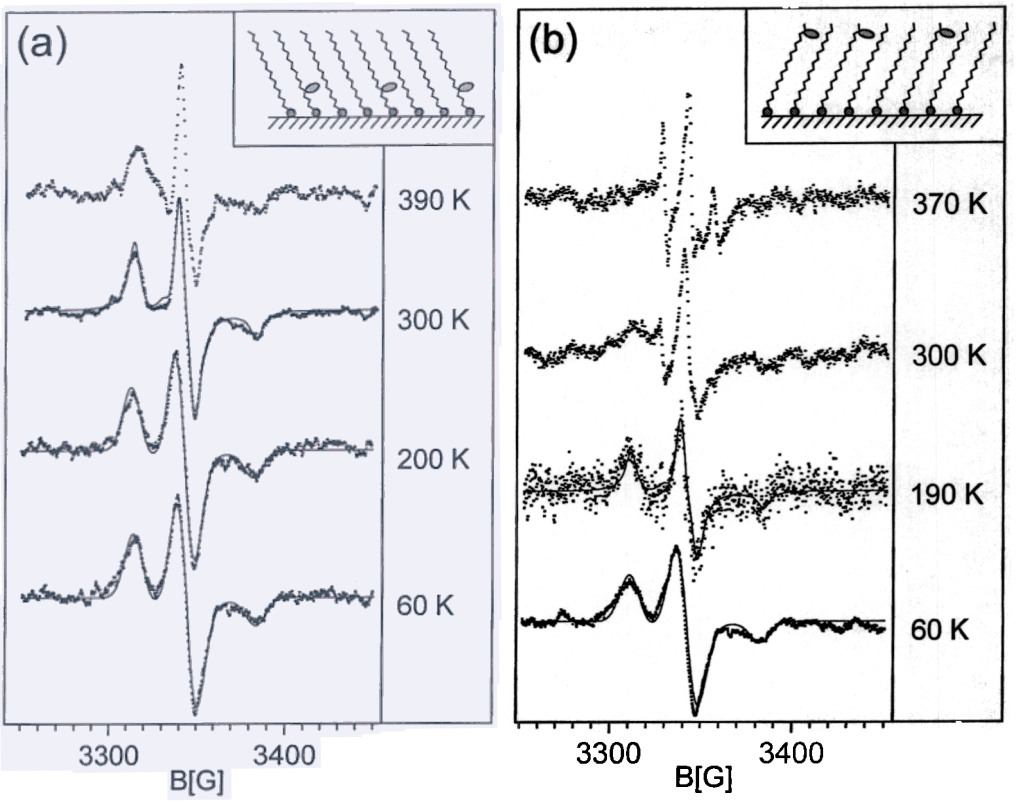

Fig. 28. Electron spin resonance spectra of 5-doxyl-stearic acid (a) and 16-doxyl-stearic acid (b) on Al_2O_3 as a function of temperature [136, 137].

sitions of the aliphatic chain, are well known as paramagnetic probes in the study of natural and synthetic membranes. The spin labeled molecules are present only as 5 % of a monolayer and are diluted with non spin labeled stearic acid molecules. Fig. 28a shows the measured temperature dependence of a SAM where the spin label is close (n = 5) to the anchoring carboxyl group of the chain to the oxide surface, while in Fig. 28b the corresponding spectra for a film with the spin label in n = 16 position, i.e. near the end of the aliphatic chain close to the vacuum interface are presented. The line shape of the spectra in Fig. 28a for temperatures up to 200 K remains unchanged whereas the intensities decrease according to Curie´s law.

Increasing the temperature to values higher than 200 K results in a decrease of the line width (see, e.g., the spectra at 60 and 300 K in Fig. 28a). However, the positions of the characteristic spectral features remain unchanged. This behavior may be interpreted in terms of very slow motion of the spin label but it is difficult to understand, because it is known from the literature [138] that the line width of the spectra should increase first before changes in line positions occur. An alternative mechanism for line broadening at low temperatures is inhomogeneous broadening due to unresolved proton superhyperfine interactions. Apart from an increasing line width, this mechanism should change the line shape from Lorentzian to Gaussian [139]. This can be shown to be the case [140]. The solid lines in Fig. 28a represent computer simulations of the spectra assuming a

rigid, randomly oriented ensemble of spin labels. Whereas the spectrum at 300 K is computed with Lorentzian lines, the spectra at 200 and 60 K are calculated using Gaussian line shapes. The change from Lorentzian to Gaussian line shape is necessary in order to fit the rigid limit spectra with a single set of g- and A-tensors. This indicates that the changes in the line width above 200 K are due to the motion of the protons in the surroundings of the spin label. On subsequent raising of the temperature higher than 315 K, the line shape changes again. But now the changes of the line shape, namely, the growth of a structure between the two maxima of the spectra, are indicative of the motion of spin labels connected to the alkyl chains themselves [141].

Turning now to the spectra in Fig. 28b with the spin label far away from the oxide surface we compare the spectrum recorded at 60 K with the corresponding spectrum in Fig. 28a. There are no pronounced differences. This behavior is expected because both spectra reflect an ensemble of static molecules. The situation changes at higher temperatures: Whereas the spectrum of 5-DXSA at 200 K could be described as a rigid limit spectrum with Gaussian line shape due to unresolved proton superhyperfine interactions, the equivalent spectrum of 16-DXSA is a rigid limit spectrum as far as the spin label is concerned, but the line shape is almost Lorentzian. The onset of the protons motion for the 16-DXSA is approximately at 140 K. This is in good agreement with helium atom scattering experiments of Scoles et al. [142] who observed a loss of the ordered structure above 100 K and attributed this effect to the motion of the terminal alkyl groups.

The two high-temperature spectra clearly indicate the motion of the spin label itself. Compared to the 5-DXSA films the motion is considerably more excited. In an attempt to understand the dynamics in terms of liquid-like motion, the increase of the rotational constants should lead to a shift of the whole structure at the high- and low-field extrema toward the isotropic values.

There is still more information in the spectra which we will not dwell upon at this point. In a recent detailed article simulations [137] including the various degrees of freedom of the chains and the constituting groups have been reported.

4. SURFACES OF OXIDES WITH RUTILE STRUCTURE

Fig. 29 shows the volume structure of rutile [15]. The sizes of the unit cells of TiO_2, VO_2 and RuO_2 are given in Fig. 29. Probably, the best studied clean oxide surfaces are the $TiO_2(100)$ and $TiO_2(110)$ surfaces. A STM image of the clean $(1x1)TiO_2(110)$ surface taken by Diebold and her group is shown in Fig. 30 [143]. It is noteworthy, that one of the first atomically resolved images of this surface was reported by Thornton and his group [144]. The inset shows a ball and stick model of the surface. There is now accumulating evidence from theoretical modeling of the tunneling conditions, but also from adsorbate studies using molecules which are assumed to bind to the exposed Ti-sites, that the bright

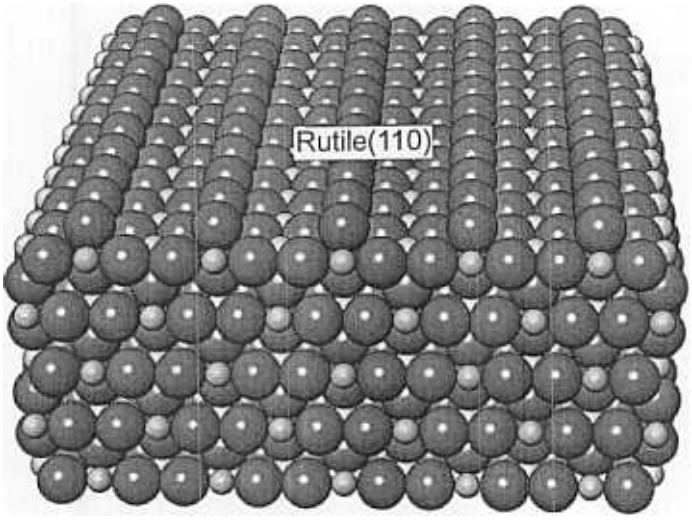

Lattice parameter for different rutile-type oxides

oxide	a	c
CrO_2	4.41	2.91
MoO_2	4.86	2.79
RuO_2	4.51	3.11
SnO_2	4.74	3.19
TiO_2	4.59	2.96
VO_2	4.55	2.85
WO_2	4.86	2.77

Fig. 29. Schematic representation of the bulk rutile unit cell (lattice parameters are given in the inset for different materials) [15, 150]

rows are representing Ti atoms. Iwasawa and his group [145-148] have successfully used formic acid in such a study, and showed in line with the theoretical predictions, and counter-intuitive with respect to topological arguments, that the Ti-ions are imaged as bright lines and the oxygen rows as dark lines. Taking the resolvable interatomic distances within the surface layer the values correspond to the structure of the charge neutral truncation of the stoichiometric (110) surface [149].

Interatomic distances normal to the surface, however, are substantially different from the bulk values as is revealed by X-ray scattering experiments [149]. The top layer six-fold coordinated Ti-atoms move outward and the five-fold-co-

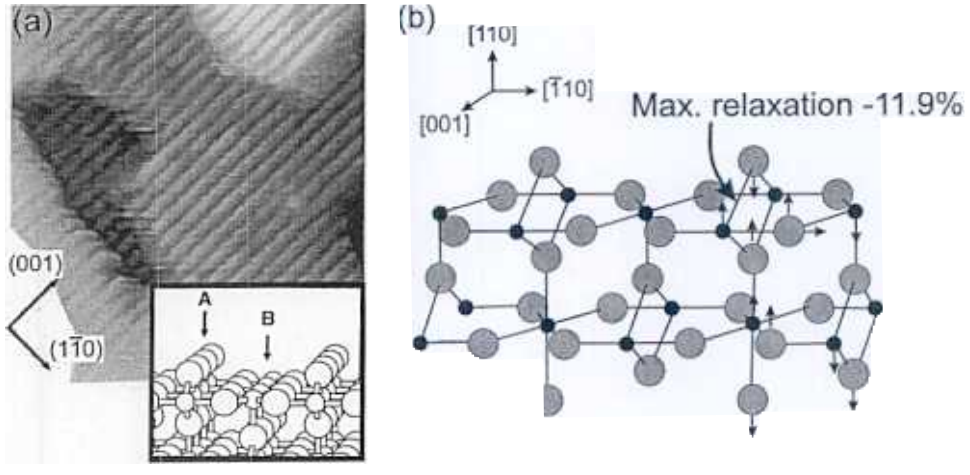

Fig. 30. Structure of the TiO_2(110) surface as determined via STM (left panel) [144] and grazing incidence X-ray scattering (right panel) [149].

ordinated Ti-atoms inward. This leads to a rumpling of 0.3 ± 0.1 Å. The rumpling repeats itself in the second layer down with an amplitude of about half of that in the top layer. Bond length variations range from 11.9 % contraction to 9.3 % expansion. These strong relaxations are not untypical for oxide surfaces and had been theoretically predicted for quite a while [8]. Recently, STM images from the $RuO_2(110)$ surface, prepared as a thin film on a Ru(0001) surface, have been reported [151]. The results are shown in Fig. 31. Here the bright rows are the oxygen atoms as demonstrated by adsorption of CO, which resides between the bright rows, indicating that in the case of RuO_2 the contrast is reversed with respect to TiO_2. A clear reasoning for the differences has not been given so far. In addition to STM the structure has been analyzed through a LEED I/V study. The surface appears to be basically bulk terminated with smaller relaxations as compared to the $TiO_2(110)$ case. Over et al. have also started to prepare other low index surfaces and LEED analysis are under way [152]. For $VO_2(110)$ grown epitaxially on a $TiO_2(110)$ surface, structural data based on photoelectron diffraction are available from the Granozzi group [153-157]. It seems that the $VO_2(110)$ surface is terminated similar to the $TiO_2(110)$ case.

Molecular adsorption has been extensively studied on $TiO_2(110)$, but very little on the corresponding RuO_2 and VO_2 surfaces. Interestingly, there is very scarce recent information on CO and NO adsorption even on $TiO_2(110)$. CO adsorption has been imaged as mentioned above for RuO_2 [151]. The molecules are residing on the Ru ions between the protruding surface oxygen rows and the binding energy is 1.2 eV. The molecules are immobile at 300 K and can be imaged with the STM. A LEED structure determination yielded a C-Ru distance of 1.95 Å and a C-O bond length of 1.13 Å. Here the bonding is thought to be in

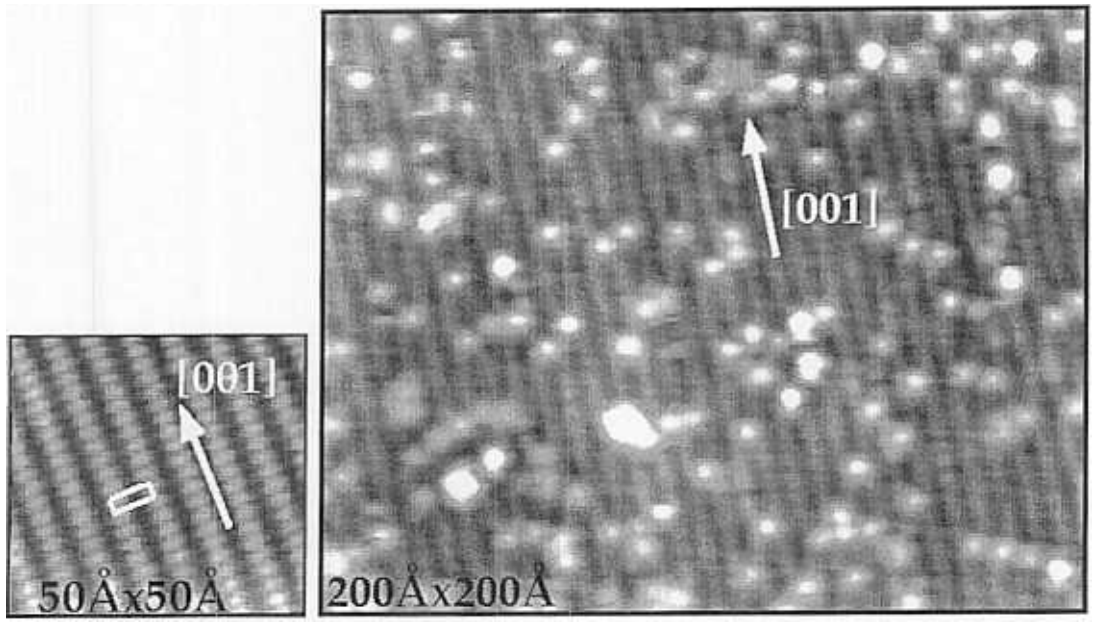

Fig. 31. Left: STM image of $RuO_2(110)$/Ru(0001) (U = -1.21 eV, I = 0.46 nA). Right: the same surface after exposure to 10 L CO (U = -1.08 eV, I = 0.46 nA). From ref. [151].

accord with the Blyholder model (Fig. 5). Upon desorption carbon dioxide is formed leaving surface oxygen vacancies behind. The oxygen is taken from the lattice and can be replenished by exposing the surface to molecular oxygen. This process of oxygen uptake by dissociating molecular oxygen from the gas phase was well known before from studies on $TiO_2(110)$, where exactly the same process applies [158]. In the latter case the extra oxygen adatoms are placed on the fivefold coordinated Ti ions.

Water adsorption has been studied quite extensively in the past, both on the $TiO_2(100)$ and the $TiO_2(110)$ surfaces [159, 160]. There is substantial evidence that water dissociates easily on the $TiO_2(100)$ surface leading to the formation of hydroxyl groups [161, 162]. On the $TiO_2(110)$ surface studies by Henderson [159] and by Hugenschmidt et al. [163] suggest that only a small fraction (from 1 % to 25 %) of the water molecules dissociates. Fig. 32 shows TDS data from Henderson's work [159]. There are basically three states of water on the surface. The low temperature peak is likely to be associated with thicker ice layers, while the peak at 175 K is due to water molecules in the second layer. The monolayer shows up as the peak shifting from close to 300 K to 270 K as a function of coverage.

Henderson [159] also investigated the vibrational properties of adsorbed water allowing the identification of monolayer and second layer water molecules through the shift of the OH stretching frequencies. Interestingly, the data suggest that the protons on the monolayer are not involved in hydrogen-bonding second

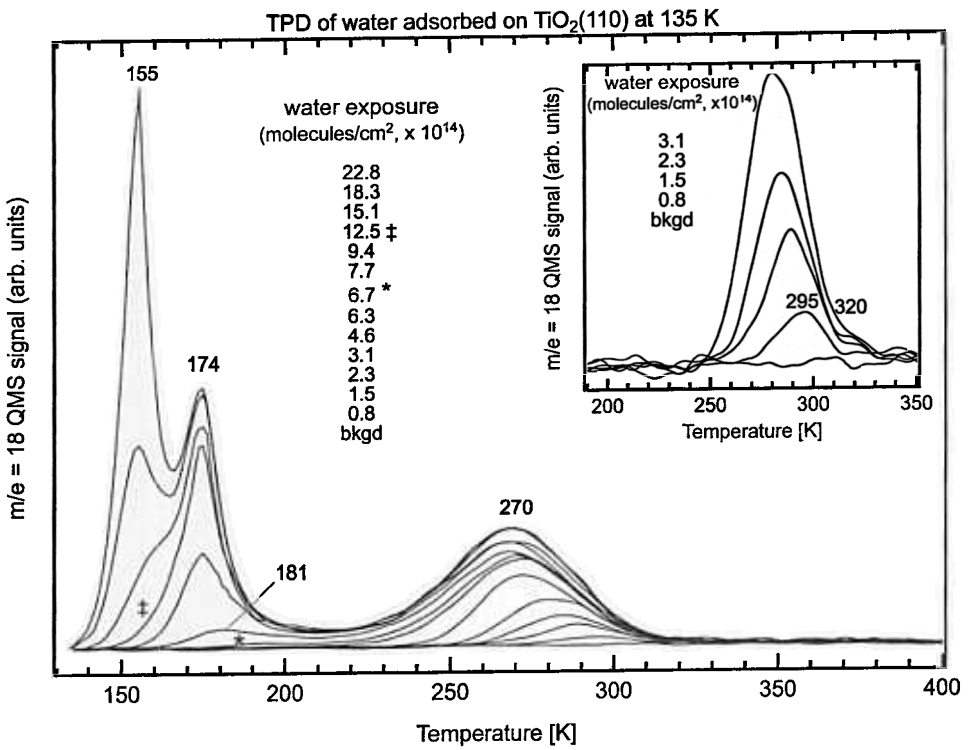

Fig. 32. Thermal desorption spectra of water desorbing from $TiO_2(110)$ after various exposures. The inset shows an enlarged plot of traces determined for low water exposures [159].

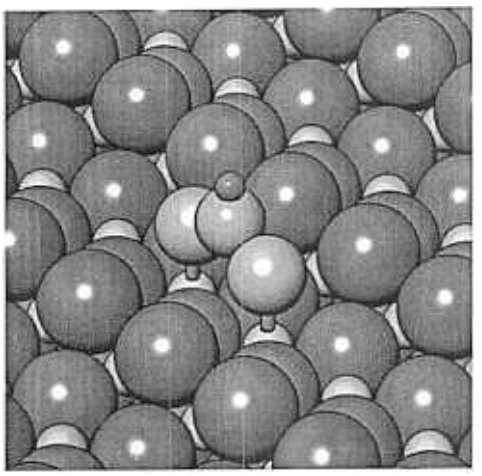

Fig. 33. Schematic representation of the geometry of adsorbed formate on $TiO_2(110)$ [165].

layer water molecules. Engel and his group [160] have recently corroborated via molecular beam studies, that, in fact, water does not dissociate on the regular $TiO_2(110)$, and that the small fraction of dissociating molecules reside on defect sites.

Another widely studied adsorption system on $TiO_2(110)$ is related to formic acid [164-166]. Upon exposure of the $TiO_2(110)$ surface to formic acid, strongly bound formate is formed, and this formate has been shown to reside on the Ti ions as already mentioned above. The protons form surface hydroxyl groups with a stretching frequency of 3605 cm^{-1}. Photoelectron diffraction studies [165] revealed the geometry of the bound formate molecule as reproduced in Fig. 33. It binds through both oxygens to pairs of neighboring Ti ions oriented along the (001) rows. The O-C-O bond angle is 126 $\pm$ 4°, and the vertical distance between formate oxygens and surface Ti ions is 2.1 $\pm$ 0.1 Å in good agreement with structure optimizations based on Hartree-Fock total energy minimization.

5. SURFACES OF OXIDES WITH LAYERED STRUCTURES

Fig. 34 shows the volume structure of vanadium-pentoxide [15]. The layered

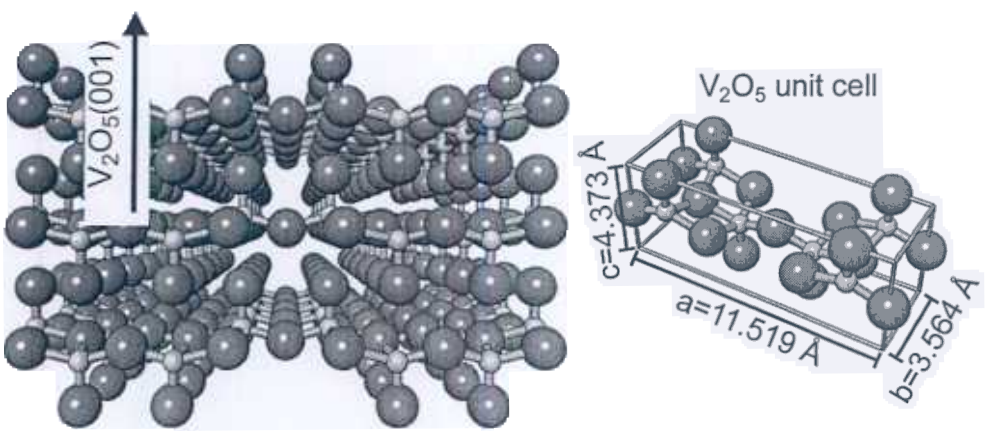

Fig. 34. Schematic representation of the bulk structure of V_2O_5 including the dimensions of the unit cell [15].

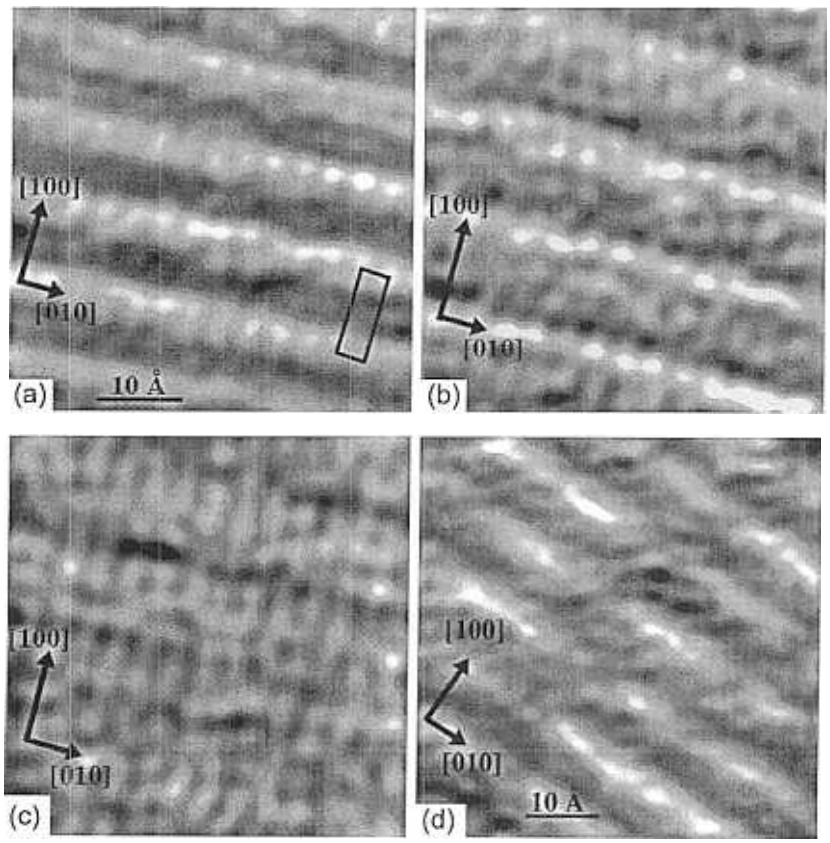

Fig. 35. Four constant current STM images of the (001) surface of Na doped V_2O_5 recorded with similar experimental parameters (U: 2-3 V, I: 0.6-1.0 nA) [167]. Images (a), (b), and (c) have the same scale and orientation. The image in (d) covers a slightly larger area and has a different orientation. The surface repeat unit is indicated by the rectangle in (a). The vertical scale from black to white is in: (a) 2.25 Å, (b) 1.5 Å, (c) 1 Å and (d) 2.25 Å.

structure of the material is quite obvious and its electronic structure has been discussed in detail on the basis of diffraction data and theoretical investigations. The material cleaves almost exclusively along the (001) surface, i.e. between the layers which are held by rather weak forces. Fig. 35 displays well resolved STM data reported for this surface [167]. The authors attribute the differences between the images to surface disorder mainly involving the surface vanadyl groups which are expected to be responsible for the bright areas in Figs. 35a, b and d.

Electron spectroscopic studies have been undertaken early on by Zhang and Henrich and by the Horn group [167-171]. The latter group, however, has been more interested in bulk than in surface properties. Fig. 36 shows a photoemission spectrum of $V_2O_5(001)$ at the top of the lower panel taken in the authors laboratory. It may be interpreted on the basis of calculations by Klaus Hermann and his group [172]. Briefly, the spectrum is dominated by O2p/O2s emissions and there is a minor admixture of the V3d wave functions in the panel showing the results of the calculations. There are no features near the Fermi energy which

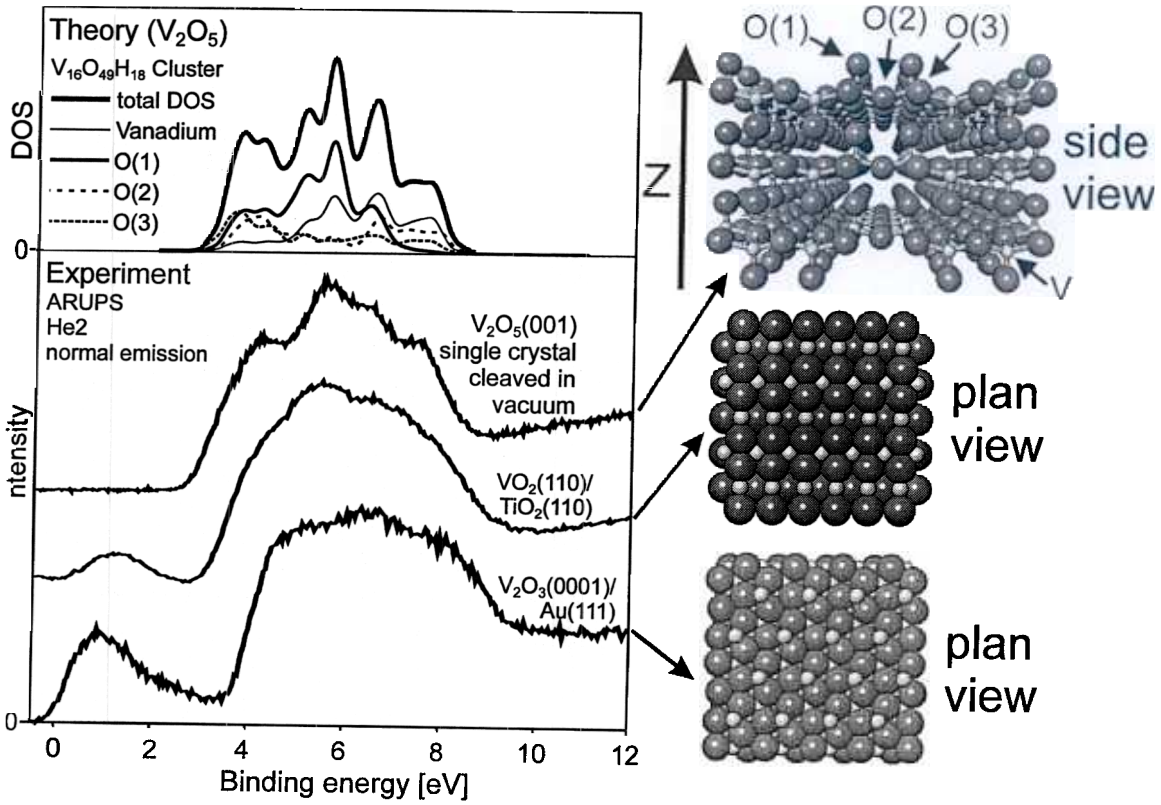

Fig. 36. Photoelectron spectra and schematic representations of structures of various vanadium oxides [98, 173]. For comparison a computed density of states [172] is shown.

would, if they were present, be characteristic for defects leaving V atoms in lower oxidation states.

The oxygen derived part of the valence band can be separated into contributions from the various types of oxygens constituting the structure as shown in the right part of Fig. 36. The terminal vanadyl oxygen {O(1)} gives rise to the central features whereas the bridging oxygens {O(2) and O(3)} connecting the vanadyl groups are contributing to the wings of the valence band. We will use this fact to identify oxygen specific reactivity.

The spectrum in the panel below V_2O_5 is that of VO_2. VO_2(110) has been grown as a thin film on the isostructural rutile(110) surface as discussed above. The oxygen derived valence band is slightly different from that of V_2O_5. A characteristic difference is the appearance of a feature close to the Fermi edge in VO_2 indicating the presence of vanadium 3d electrons. Its intensity represents to some extent the population of the V3d orbitals. When we turn from VO_2 to V_2O_3 (also discussed above) an even stronger increase in the V3d intensity is observed. In Fig. 36, in the lower panel, the valence band photoemission spectrum of V_2O_3(0001)/Au(111), is shown. The V_2O_3 film shows a sharp hexagonal LEED [98] pattern (see Fig. 16) representing the corundum type structure similar to Al_2O_3, Cr_2O_3 and Fe_2O_3 (see above). Again, the V_2O_3 oxygen valence band emission is not very characteristic, as compared with VO_2 and

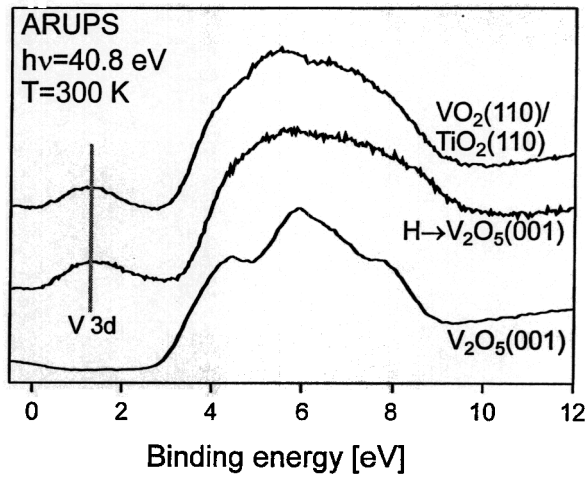

Fig. 37. Photoelectron spectra of $V_2O_5(001)$ and $VO_2(110)/TiO_2(110)$ in comparison with a photoelectron spectrum obtained after dosing atomic hydrogen to a $V_2O_5(001)$ surface.

V_2O_5. It is only the change in the near Fermi edge structures that show a characteristic variation from V^{5+} to V^{3+}.

Vanadium pentoxide is rather inactive with respect to adsorbates. For example, molecular hydrogen only leads to observable effects in the photoelectron spectrum after 10^4 L exposure, On the other hand, atomic hydrogen leads already at low exposure to recognizable changes in the photoelectron spectrum. The spectrum shown in Fig. 37 in the middle has been obtained after exposing the surface to atomic hydrogen. Opposite to the finding with molecular hydrogen the surface is chemically corroded. Defects form, as we also know from electron energy loss spectroscopy, and concomitantly reduced metal centers show up near the Fermi edge. In fact, the spectrum looks very similar to the one of VO_2 which we show for comparison. We have investigated the surface with vibrational spectroscopy and found no indication for the formation of hydroxyls. It is very likely, that during exposure water evolves from the surface. Still the complete absence of OH on the surface is surprising and might point to the formation of hydrogen vanadium oxide bronzes which are well-known to exist and which also have been used as precursors in the preparation of catalysts [174].

6. SYNOPSIS

The present review has been focussed on discussing the geometric and electronic properties of surfaces as related to their ability to adsorb and electronically modify molecules. Still this field is in its infancy for oxide surfaces when compared to vast amount of data available for metal surfaces. It is important to recognize, that the interaction of molecules with oxide surfaces has to be compared with care with the established bonding models for metal surfaces. This fact, although quite obvious is not always properly appreciated. For oxide surfaces electrostatic effects have to be taken into account, especially for the highly ionic materials. For example, even though CO binds to MgO or NiO in the same

geometry as on a metal surface, the synergetic σ-bonding-π-backbonding mechanism (Blyholder model) cannot be appropriately used to understand the bonding. Other oxides, which have more covalent bonding character, may, on the other hand, be properly described using such models. RuO_2 seems to be an example. In general, water adsorption has been studied to a large extent due to its importance in geochemical and electrochemical studies. While information for the well ordered and carefully prepared surfaces is accumulating, it becomes more and more important to try to understand the nature of well identified defects on the adsorption properties. In the field of oxide surface chemistry research, it is the belief of the authors, that this field will be an interesting but also a challenging one, if well characterized systems are used.

REFERENCES

[1] H. Schmalzried, Chemical Kinetics of Solids, (Verlag Chemie, Weinheim, 1995).
[2] V.E. Henrich and P.A. Cox, The Surface Science of Metal Oxides, (Cambridge University Press, Cambridge, 1994).
[3] C. Xu and D.W. Goodman, in Handbook of Heterogeneous Catalysis, edited by G. Ertl, H. Knözinger, and J. Weitkamp, Vol. 2 (Wiley-VCH, Weinheim, 1997), page 826.
[4] S.C. Street and D.W. Goodman, in Growth and Properties of Ultrathin Epitaxial Layers, The Chemical Physics of Solid Surfaces, edited by D. A. King and D. P. Woodruff, Vol. 8 (Elsevier, New York, 1997), page 375.
[5] R.J. Lad, Surf. Rev. Lett., 2 (1995) 109.
[6] H.-J. Freund, H. Kuhlenbeck and V. Staemmler, Rep. Progr. Phys., 59 (1996) 283.
[7] H. Kuhlenbeck and H.-J. Freund, in Growth and Properties of Ultrathin Epitaxial Layers, The Chemical Physics of Solid Surfaces, edited by D. A. King and D. P. Woodruff, Vol. 8 (Elsevier, New York, 1997), page 340.
[8] G. Renaud, Surf. Sci. Rep., 32 (1998) 1.
[9] C.A. Ventrice and H. Geisler, in Thin Films: Heteroepitaxial Systems, (Chapter 4), edited by A. W. K. Liu and M. B. Santos (World Scientific, Singapore, 1999).
[10] H.-J. Freund, Faraday Disc., 114 (1999) 1.
[11] S.A. Chambers, Surf. Sci. Rep., 39 (2000) 105.
[12] R. Franchy, Surf. Sci. Rep., 38 (2000) 195.
[13] C. Noguera, Physics and Chemistry at Oxide Surfaces, (Cambridge University Press, Cambridge, 1996).
[14] P.W. Tasker, Adv. Ceram., 10 (1984) 176.
[15] R.W.G. Wyckoff, Crystal Structures, (Wiley Interscience, New York, 1965).
[16] K.O. Legg, M. Prutton and C. Kinniburgh, J. Phys. C: Solid State Phys., 7 (1974) 4236.
[17] D.L. Blanchard, D.L. Lessor, J.P. LaFemina, D.R. Baer, F. W.K. and T. Guo, J. Vac. Sci. Technol. A, 9 (1991) 1814.
[18] K.H. Rieder, Surf. Sci. Lett., 118 (1982) 57.
[19] M. Prutton, J.A. Walker, M.R. Welton-Cook, R.C. Felton and J.A. Ramsey, Surf. Sci. Lett., 89 (1979) 95.
[20] F.P. Netzer and M. Prutton, J. Phys. C: Solid State Phys., 8 (1975) 2401.
[21] C.G. Kinniburgh and J.A. Walker, Surf. Sci., 63 (1977) 274.
[22] M.R. Castell, C. Muggelberg, S.L. Dudarev, A.P. Sutton, G.A.D. Briggs and D.T. Goddard, Appl. Phys. A, 66 (1998) S963.

[23] M.R. Castell, P.L. Wincott, N.G. Condon, C. Muggelberg, G. Thornton, S.L. Dudarev, A.P. Sutton and G.A.D. Briggs, Phys. Rev. B, 55 (1997) 7859.
[24] H. Hosoi, K. Sueoka, K. Hayakawa and K. Mukasa, Appl. Surf. Sci., 157 (2000) 218.
[25] M.R. Castell, S.L. Dudarev, G.A.D. Briggs and A.P. Sutton, Phys. Rev. B, 59 (1999) 7342.
[26] C. Noguera, A. Pojani, F. Finocchi and J. Goniakowski, in Chemisorption and Reactivity on Supported Clusters and Thin Films, edited by R. M. Lambert and G. Pacchioni, NATO ASI Series E, Vol. 331 (Kluwer Academic Publishers, Dordrecht, 1997), page 445.
[27] D. Wolf, Phys. Rev. Lett., 68 (1992) 3315.
[28] F. Rohr, K. Wirth, J. Libuda, D. Cappus, M. Bäumer and H.-J. Freund, Surf. Sci., 315 (1994) L977.
[29] A. Barbier and G. Renaud, Surf. Sci., 392 (1997) L15.
[30] A. Barbier, in Proceedings of the 1st International Workshop on Oxide Surfaces, (Elmau, Germany, 1999).
[31] A. Barbier, C. Mocuta, H. Kuhlenbeck, K.F. Peters, B. Richter and G. Renaud, Phys. Rev. Lett., 84 (2000) 2897.
[32] C.A. Ventrice Jr., T. Bertrams, H. Hannemann, A. Brodde and H. Neddermeyer, Phys. Rev., B49 (1994) 5773.
[33] V.E. Henrich, Surf. Sci., 57 (1976) 385.
[34] O. Robach, G. Renaud and A. Barbier, Surf. Sci., 401 (1998) 227.
[35] S. Hüfner, P. Steiner, I. Sander, M. Neumann and S. Witzel, Z. Phys. B, 83 (1991) 185.
[36] S. Hüfner, Photoelectron Spectroscopy: Principles and Applications, (Springer-Verlag, Berlin, 1995).
[37] C. Noguera and W.C. Mackrodt, J. Phys. Condens. Matter, 12 (2000) 2163.
[38] W.C. Mackrodt and C. Noguera, Surf. Sci., 457 (2000) L386.
[39] A. Gorschlüter and H. Merz, Phys. Rev. B, 49 (1994) 17293.
[40] A. Freitag, V. Staemmler, D. Cappus, C.A. Ventrice Jr., K. Al-Shamery, H. Kuhlenbeck and H.-J. Freund, Chem. Phys. Lett., 210 (1993) 10.
[41] R. Newman and R.M. Chrenko, Phys. Rev., 114 (1959) 1507.
[42] R.J. Powell, Report 5220-1 Stanford Electronics Laboratory, 1967.
[43] D. Adler and J. Feinleib, Phys. Rev. B, 2 (1970) 3112.
[44] B. Fromme, M. Möller, T. Anschütz, C. Bethke and E. Kisker, Phys. Rev. Lett., 77 (1996) 1548.
[45] B. Fromme, C. Koch, R. Deussen and E. Kisker, Phys. Rev. Lett., 75 (1995) 693.
[46] M. Pöhlchen and V. Staemmler, J. Chem. Phys., 97 (1992) 2583.
[47] F. Müller, R. de Masi, P. Steiner, D. Reinicke, M. Stadtfeld and S. Hüfner, Surf. Sci., 459 (2000) 161.
[48] M. Henzler and W. Göpel, Oberflächenphysik des Festkörpers, (Teubner-Verlag, Stuttgart, 1991).
[49] K.M. Neyman, G. Pacchioni and N. Rösch, in Recent Developments and Applications of Modern Density Functional Theory and Computational Chemistry, edited by J. M. Seminario (Elsevier, Amsterdam, 1996), page 569.
[50] H.-J. Freund, Angew. Chem. Int. Ed. Engl., 36 (1997) 452.
[51] M. Bäumer, J. Libuda and H.-J. Freund, in Chemisorption and Reactivity on Supported Clusters and Thin Films, edited by R. M. Lambert and G. Pacchioni, NATO ASI Series E, Vol. 331 (Kluwer Academic Press, Dordrecht, 1997), page 61.
[52] M.A. Nygren and L.G.M. Pettersson, J. Chem. Phys., 105 (1996) 9339.

[53] G. Pacchioni and P.S. Bagus, in Adsorption on Ordered Surfaces of Ionic Solids and Thin Films, edited by H.-J. Freund and E. Umbach, Springer Series in Surface Science, Vol. 33 (Springer Verlag, Berlin, 1993), page 180.
[54] T. Klüner, private communication.
[55] D. Cappus, J. Klinkmann, H. Kuhlenbeck and H.-J. Freund, Surf. Sci., 325 (1995) L 421.
[56] S.M. Vesecky, X. Xu and D.W. Goodman, J. Vac. Sci. Technol. A, 12 (1994) 2114.
[57] V. Staemmler, in Adsorption on Ordered Surfaces of Ionic Solids and Thin Films, edited by H.-J. Freund and E. Umbach, Springer Series in Surface Science, Vol. 33 (Springer Verlag, Berlin, 1993), page 169.
[58] M. Pöhlchen, PhD Thesis, Ruhr-Universität Bochum, 1992.
[59] H. Kuhlenbeck, G. Odörfer, R. Jaeger, G. Illing, M. Menges, T. Mull, H.-J. Freund, M. Pöhlchen, V. Staemmler, S. Witzel, C. Scharfschwerdt, K. Wennemann, T. Liedtke and M. Neumann, Phys. Rev. B, 43 (1991) 1969.
[60] L. Chen, R. Wu, N. Kioussis and Q. Zhang, Chem. Phys. Lett., 290 (1998) 255.
[61] K.M. Neyman, S.P. Ruzankin and N. Rösch, Chem. Phys. Lett., 246 (1995) 546.
[62] J.-W. He, C.A. Estrada, J.S. Corneille, M.-C. Wu and D.W. Goodman, Surf. Sci., 261 (1992) 164.
[63] S. Furuyama, H. Fuji, M. Kawamura and T. Morimoto, J. Phys. Chem., 82 (1978) 1028.
[64] R. Wichtendahl, M. Rodriguez-Rodrigo, U. Härtel, H. Kuhlenbeck and H.-J. Freund, phys. stat. sol. (a), 173 (1999) 93.
[65] P.A. Redhead, Vacuum, 12 (1962) 203.
[66] H. Pfnür, P. Feulner and D. Menzel, J. Chem. Phys., 79 (1983) 4613.
[67] C.N. Chittenden, E.D. Pylant, A.L. Schwaner and J.M. White, Thermal Desorption and Mass Spectrometry, (CRC Press, Boca Raton, 1995).
[68] H. Schlichting and D. Menzel, Rev. Sci. Instrum., 64 (1993) 2013.
[69] R. Lindsay, P. Baumgärtel, R. Terborg, O. Schaff, A.M. Bradshaw and D.P. Woodruff, Surf. Sci., 425 (1999) L401.
[70] K. Hermann and P.S. Bagus, Phys. Rev. B, 15 (1977) 4195.
[71] H.-J. Freund and E.W. Plummer, Phys. Rev. B, 23 (1981) 4859.
[72] E. Umbach, Surf. Sci., 117 (1982) 482.
[73] J. Heidberg, M. Kandel, D. Meine and U. Wildt, Surf. Sci., 333 (1995) 1467.
[74] R. Gerlach, A. Glebov, G. Lange, J.P. Toennies and H. Weiss, Surf. Sci., 331-333 (1995) 1490.
[75] J. Heidberg, B. Redlich and D. Wetter, Ber. Bunsenges. Phys. Chem., 99 (1995) 1333.
[76] D. Ferry, A. Glebov, V. Senz, J. Suzanne, J.P. Toennies and H. Weiss, J. Chem. Phys., 105 (1996) 1697.
[77] A. Marmier, P.N.M. Hoang, S. Picaud, C. Girardet and R.M. Lynden-Bell, J. Chem. Phys., 109 (1988) 3245.
[78] M.J. Stirniman, C. Huang, R.C. Smith, J.A. Joyce and B.D. Kay, J. Chem. Phys., 105 (1996) 1295.
[79] C. Xu and D.W. Goodman, Chem. Phys. Lett., L65 (1997) 341.
[80] R. Wichtendahl, PhD-Thesis, Freie Universität Berlin, 1999.
[81] C.M. Truong, M.-C. Wu and D.W. Goodman, J. Am. Chem. Soc., 115 (1993) 3647.
[82] C.M. Truong, M.-C. Wu and D.W. Goodman, J. Chem. Phys., 97 (1992) 9447.
[83] M.-C. Wu, C.M. Truong and D.W. Goodman, J. Phys. Chem., 97 (1993) 4182.
[84] S.C. Street, Q. Guo, C. Xu and D.W. Goodman, J. Phys. Chem., 100 (1996) 17599.
[85] A. Kara, S. Durukanoglu and T.S. Rahman, Phys. Rev. B, 53 (1996) 15489.

[86] K. Domen, N. Akamatsu, H. Yamamoto, A. Wada and C. Hirose, Surf. Sci., 283 (1993) 468.
[87] A. Bandara, J. Kubota, A. Wada, K. Domen and C. Hirose, Surf. Sci. Lett., 364 (1996) L580.
[88] A. Bandara, J. Kubota, A. Wada, K. Domen and C. Hirose, J. Phys. Chem. B, 101 (1997) 361.
[89] W.L. Roth, J. Appl. Phys., 31 (1960) 2000.
[90] H.P. Rooksby, Acta Cryst., 1 (1948) 226.
[91] S. Greenwald and J.S. Smart, Nature, 166 (1950) 523.
[92] X.-G. Wang, W. Weiss, S.K. Shaikhoutdinov, M. Ritter, M. Petersen, F. Wagner, R. Schlögl and M. Scheffler, Phys. Rev. Lett., 81 (1998) 1038.
[93] I. Manassidis and M.J. Gillan, J. Am. Ceram. Soc., 77 (1994) 335.
[94] F. Rohr, M. Bäumer, H.-J. Freund, J.A. Mejias, V. Staemmler, S. Müller, L. Hammer and K. Heinz, Surf. Sci., 372 (1997) L 291.
[95] F. Rohr, M. Bäumer, H.-J. Freund, J.A. Mejias, V. Staemmler, S. Müller, L. Hammer and K. Heinz, Surf. Sci., 389 (1997) 391.
[96] S.K. Shaikhoutdinov and W. Weiss, Surf. Sci., 432 (1999) L627.
[97] K.B. Lewis, S.T. Oyama and G.A. Somorjai, Surf. Sci., 233 (1990) 75.
[98] A.-C. Dupuis, PhD-Thesis, in preparation.
[99] N.M. Harrison, X.-G. Wang, J. Muscat and M. Scheffler, Faraday Disc., 114 (1999) 305.
[100] K. Wolter, D. Scarano, J. Fritsch, H. Kuhlenbeck, A. Zecchina and H.-J. Freund, Chem. Phys. Lett., 105 (2000) 295.
[101] B. Dillmann, F. Rohr, O. Seiferth, G. Klivenyi, M. Bender, K. Homann, I.N. Yakovkin, D. Ehrlich, M. Bäumer, H. Kuhlenbeck and H.-J. Freund, Faraday Disc. 105, (1996) 295.
[102] C. Xu, M. Haßel, H. Kuhlenbeck and H.-J. Freund, Surf. Sci., 258 (1991) 23.
[103] M.A. Henderson and S.A. Chambers, Surf. Sci., 449 (2000) 135.
[104] J.A. Mejias, V. Staemmler and H.-J. Freund, J. Phys. Cond. Matter, 11 (1999) 7881.
[105] H. Kuhlenbeck, C. Xu, B. Dillmann, M. Haßel, B. Adam, D. Ehrlich, S. Wohlrab, H.-J. Freund, U.A. Ditzinger, H. Neddermeyer, M. Neuber and M. Neumann, Ber. Bunsenges. Phys. Chem., 96 (1992) 15.
[106] C. Xu, B. Dillmann, H. Kuhlenbeck and H.-J. Freund, Phys. Rev. Lett., 67 (1991) 3551.
[107] M. Bender, D. Ehrlich, I.N. Yakovkin, F. Rohr, M. Bäumer, H. Kuhlenbeck, H.-J. Freund and V. Staemmler, J. Phys. Cond. Matter, 7 (1995) 5289.
[108] M. Pykavy, V. Staemmler, O. Seiferth and H.-J. Freund, Surf. Sci., (submitted).
[109] M.A. Henderson, S.A. Joyce and J.R. Rustad, Surf. Sci., 417 (1998) 66.
[110] P. Lin, T. Kendelewicz, G.E. Brown, E.J. Nelson and S.A. Chambers, Surf. Sci., 417 (1998) 53.
[111] D. Ehrlich, PhD-Thesis, Ruhr-Universität Bochum, 1995.
[112] O. Seiferth, K. Wolter, B. Dillmann, G. Klivenyi, H.-J. Freund, D. Scarano and A. Zecchina, Surf. Sci., 421 (1999) 176.
[113] V. Coustet and J. Jupille, Surface and Interface Analysis, 22 (1994) 280.
[114] V. Coustet and J. Jupille, Surf. Sci., 307-309 (1994) 1161.
[115] K.C. Haas, W.F. Schneider, A. Curloni and W. Andreoni, Science, 282 (1998) 265.
[116] J. Libuda, M. Frank, A. Sandell, S. Andersson, P.A. Brühwiler, M. Bäumer, N. Mårtensson and H.-J. Freund, Surf. Sci., 384 (1997) 106.
[117] A. Zecchina, D. Scarano, S. Bordiga, G. Ricchiardi, G. Spoto and F. Geobaldo, Catal. Today, 27 (1996) 403.

[118] I. Hemmerich, F. Rohr, O. Seiferth, B. Dillmann and H.-J. Freund, Z. Phys. Chem., 202 (1997) 31.
[119] P.C. Thüne and J.W. Niemantsverdriet, Israel. J. Chem., 38 (1998) 385.
[120] 12th International Congress on Catalysis, Studies in Surface Science and Catalysis, edited by A. Corma, F.V. Melo, S. Mendioroz and J.L.G. Fierro (Elsevier, Amsterdam, 2000).
[121] H. Schlienz, M. Beckendorf, U.J. Katter, T. Risse and H.-J. Freund, Phys. Rev. Lett., 74 (1995) 761.
[122] M.E. Bartram and B.E. Koel, Surf. Sci., 213 (1989) 137.
[123] U.J. Katter, H. Schlienz, M. Beckendorf and H.-J. Freund, Ber. Bunsenges. Phys. Chem., 97 (1993) 340.
[124] Principles of Electron Spin Resonance, edited by N.M. Atherton (Ellis Horwood PTR Prentice Hall, New York, 1993).
[125] A. Abragam and B. Bleaney, in Electron Paramagnetic Resonance of Transition Ions (Clarendon Press, Oxford, 1970), page 492.
[126] P.G. Gray and A.D. Yoffe, Chem. Rev., 55 (1955) 1069.
[127] M. Beckendorf, U.J. Katter, H. Schlienz and H.-J. Freund, J. Phys. Condens. Matter, 5 (1993) 5471.
[128] M. Beckendorf, PhD-Thesis, Ruhr-Universität Bochum, 1994.
[129] D.L. Freeman and J.D. Doll, J. Chem. Phys., 78 (1983) 6002.
[130] B. Roop, S.A. Costello, D.R. Mullins and J.M. White, J. Chem. Phys., 86 (1987) 3003.
[131] U.J. Katter, T. Hill, T. Risse, H. Schlienz, M. Beckendorf, T. Klüner, H. Hamann and H.-J. Freund, J. Phys. Chem. B, 101 (1997) 3776.
[132] G. Poggi and C.S. Johnson, Jr., J. Magn. Reson., 3 (1970) 436.
[133] U.J. Katter, T. Hill, T. Risse, H. Schlienz, M. Beckendorf, T. Klüner, H. Hamann and H.-J. Freund, J. Phys. Chem. B, 101 (1997) 552.
[134] P.A. Egelstaff, J. Chem. Phys., 53 (1970) 2590.
[135] G.L. Millhauser and J.H. Freed, J. Chem. Phys., 81 (1984) 37.
[136] T. Risse, T. Hill, M. Beckendorf, U.J. Katter, H. Schlienz, H. Hamann and H.J. Freund, Langmuir, 12 (1996) 5512.
[137] T. Risse, T. Hill, J. Schmidt, G. Abend, H. Hamann and H.-J. Freund, J. Chem. Phys., 108 (1998) 8615.
[138] J.H. Freed, G.V. Bruno and C.F. Polnaszek, J. Phys. Chem., 75 (1971) 3385.
[139] B.L. Bales, in Spin Labeling Theory and Applications: Biological Magnetic Resonance, edited by L. J. Berliner and J. Reuben, Vol. 8 (Plenum Press, New York, 1989), page 77.
[140] T. Risse, PhD-Thesis, Ruhr-Universität Bochum, 1996.
[141] M. Ge and J.H. Freed, Biophys. J., 65 (1993) 2106.
[142] C.E.D. Chidsey, G.-L. Liu, P. Rowntree and G. Scoles, J. Chem. Phys., 91 (1989).
[143] U. Diebold, J.F. Anderson, K.-O. Ng and D. Vanderbilt, Phys. Rev. Lett., 77 (1996) 1322.
[144] P.W. Murray, N.G. Condon and G. Thornton, Phys. Rev. B, 51 (1995) 10989.
[145] H. Onishi and Y. Iwasawa, Surf. Sci., 313 (1994) L783.
[146] H. Onishi and Y. Iwasawa, Chem. Phys. Lett., 226 (1994) 111.
[147] H. Onishi, K. Fukui and Y. Iwasawa, Bull. Chem. Soc. Jpn., 68 (1995) 2447.
[148] H. Onishi and Y. Iwasawa, Phys. Rev. Lett., 76 (1996) 791.
[149] G. Charlton, P.B. Howes, C.L. Nicklin, P. Steadman, J.S.G. Taylor, C.A. Muryn, S.P. Harte, J. Mercer, R. McGrath, D. Norman, T.S. Turner and G. Thornton, Phys. Rev. Lett., 78 (1997) 495.

[150] D.B. McWhan, P.D. Dernier, M. M. Marezio and J.P. Remeika, Phys. Rev. B, 10 (1974).
[151] H. Over, Y.D. Kim, A.P. Seitsonen, S. Wendt, E. Lundgren, M. Schmid, P. Varga, A. Morgante and G. Ertl, Science, 287 (2000) 1474.
[152] H. Over, private communication.
[153] P.J. Møller, Z.S. Li, T. Egebjerg, M. Sambi and G. Granozzi, Surf. Sci., 402-404 (1998) 719.
[154] M. Sambi, G. Sangiovanni, G. Granozzi and F. Parmigiani, Phys. Rev. B, 54 (1996) 13464.
[155] M. Sambi, E. Pin, G. Sangiovanni, L. Zaratin, G. Granozzi and F. Parmigiani, Surf. Sci., 349 (1996) L169.
[156] M. Sambi, G. Sangiovanni, G. Granozzi and F. Parmigiani, Phys. Rev. B, 55 (1997) 7850.
[157] M. Sambi, M.D. Negra, G. Granozzi, Z.S. Li, J.H. Jorgensen and P.J. Møller, Appl. Surf. Sci., 142 (1999) 146.
[158] W.S. Epling, C.H.F. Peden, M.A. Henderson and U. Diebold, Surf. Sci., 412/413 (1998) 333.
[159] M.A. Henderson, Surf. Sci., 355 (1996) 151.
[160] D. Brinkley, M. Dietrich, T. Engel, P. Farrall, G. Gantner, A. Schafer and A. Szuchmacher, Surf. Sci., 395 (1998) 292.
[161] M.A. Henderson, Surf. Sci., 319 (1994) 315.
[162] P.B. Smith and S. Bernasek, Surf. Sci., 188 (1988) 241.
[163] M.B. Hugenschmidt, C. Janicke and C.T. Campbell, Surf. Sci., 302 (1994) 329.
[164] Y. Iwasawa, Surf. Sci., 402-404 (1998) 8.
[165] S. Thevuthasan, G.S. Herman, Y.J. Kim, S.A. Chambers, C.H.F. Peden, Z. Wang, R.X. Ynzunza, E.D. Tober, J. Morais and C.S. Fadley, Surf. Sci., 401 (1998) 261.
[166] S.A. Chambers, M.A. Henderson, Y.J. Kim and S. Thevuthasan, Surf. Rev. Lett., 5 (1998) 381.
[167] R.L. Smith, W. Lu and G.S. Rohrer, Surf. Sci., 322 (1995) 293.
[168] T. Oshio, Y. Sakai, T. Moriya and S. Ehara, Scanning Microscopy, 7 (1993) 33.
[169] R.L. Smith, G.S. Rohrer, K.S. Lee, D.-K. Seo and M.-H. Whangbo, Surf. Sci., 367 (1996) 87.
[170] R.A. Goschke, K. Vey, M. Maier, U. Walter, E. Goering, M. Klemm and S. Horn, Surf. Sci., 438 (1996) 305.
[171] Z. Zhang and V.E. Henrich, Surf. Sci., 321 (1994) 133.
[172] K. Hermann, M. Witko, R. Druzinic, A. Chakrabarti, B. Tepper, M. Elsner, A. Gorschlüter, H. Kuhlenbeck and H.-J. Freund, J. Electron Spectrosc. Relat. Phenom., 98-99 (1999) 245.
[173] B. Tepper, PhD-Thesis, in preparation.
[174] M. Figlarz, Progr. Solid State Chem., 19 (1989) 1.